AD-A070 770 ENVIRONMENTAL RESEARCH INST OF MICHIGAN ANN ARBOR AP--ETC F/G 17/8
BASIC REMOTE SENSING INVESTIGATION FOR COASTAL RECONNAISSANCE.(U)
JUN 79 D LYZENGA, R SHUCHMAN, C DAVIS N00014-78-C-0458
UNCLASSIFIED ERIM-134400-7-T NL

1 OF 1
AD A070770

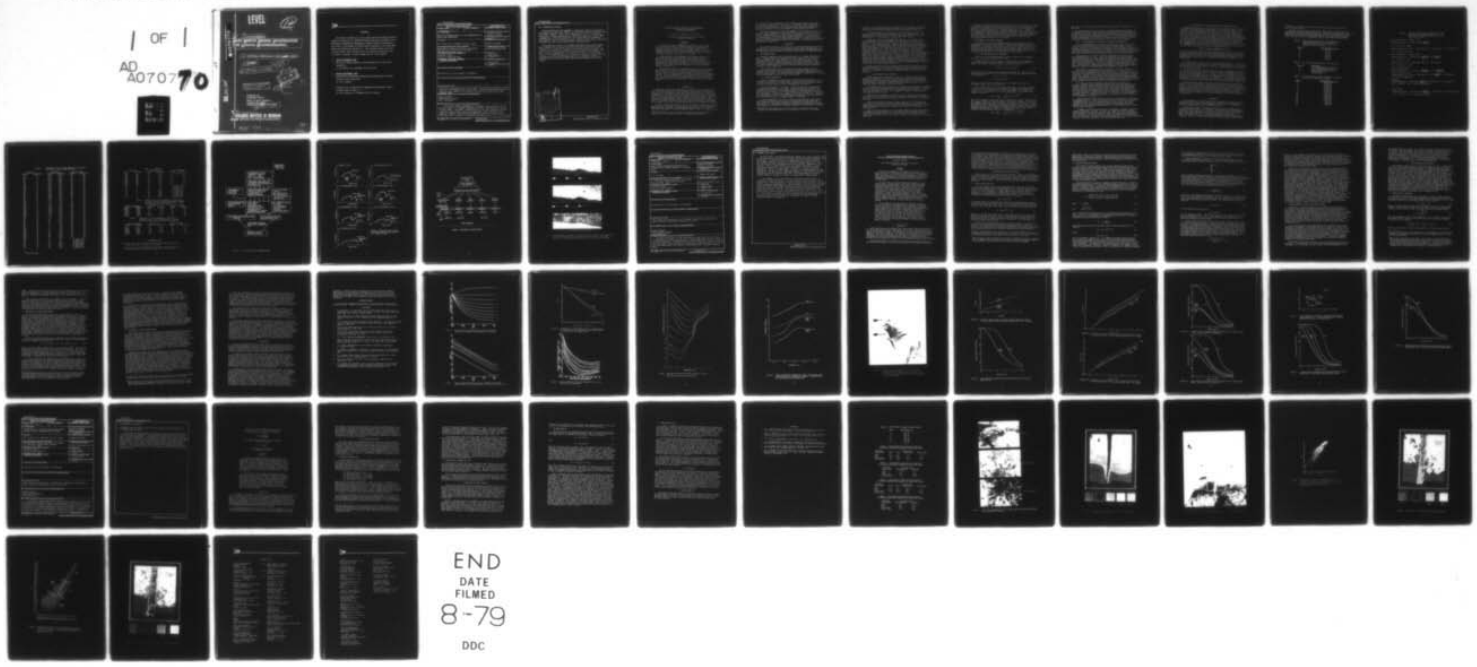

END
DATE FILMED
8-79
DDC

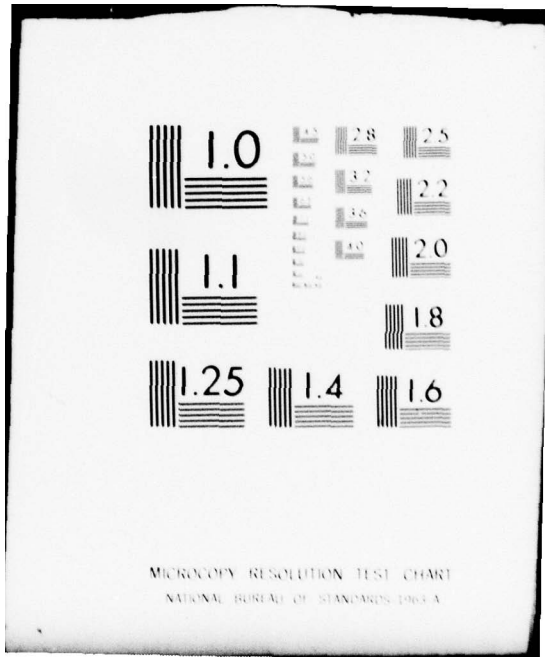
1.0
1.1
1.25
1.4
1.6
2.8
3.2
3.6
4.0
2.5
2.2
2.0
1.8
MICROCOPY RESOLUTION TEST CHART
NATIONAL BUREAU OF STANDARDS 1963 A

LEVEL II

AD A070770

DDC FILE COPY

(6) (9) Technical Report

BASIC REMOTE SENSING INVESTIGATION FOR COASTAL RECONNAISSANCE

(10) D. LYZENGA, R. SHUCHMAN, C. DAVIS [redacted] G. SUITS

(11) JUNE 1979 (12) 58p.

(14) ERIM-134400-7-T

Prepared for:
Geography Branch

Office of Naval Research
Arlington, VA 22217
Contract No. N00014-78-C-0458
(15)

ENVIRONMENTAL
RESEARCH INSTITUTE OF MICHIGAN
FORMERLY WILLOW RUN LABORATORIES, THE UNIVERSITY OF MICHIGAN
BOX 8618 • ANN ARBOR • MICHIGAN 48107

JOB

410 937

ERIM

CONTENTS

This report consists of a set of three papers describing technical progress on Contract No. N00014-78-C-0458, which were presented at the Thirteenth International Symposium on Remote Sensing of Environment. The titles of the papers are listed below according to the tasks under which the research was carried out. The technical monitor for this contract was Mr. Hans Dolezalek, and the principal investigator was Dr. David R. Lyzenga. Project manager was Mr. Fred Thomson.

1. BEACH ENVIRONMENT TASK:

   The Use of Remote Sensing in the Determination of Beach Sand Parameters

   by C.F. Davis, R.A. Shuchman, and G.H. Suits

2. MARINE ENVIRONMENT TASK:

   Shallow-Water Reflectance Modeling with Applications to Remote Sensing of the Ocean Floor

   by D.R. Lyzenga

   Evaluation of an Algorithm for Mapping Bottom Features Under a Variable Depth of Water.

   by D.R. Lyzenga, R.A. Shuchman, and R.A. Arnone

UNCLASSIFIED

SECURITY CLASSIFICATION OF THIS PAGE (When Data Entered)

REPORT DOCUMENTATION PAGE		READ INSTRUCTIONS BEFORE COMPLETING FORM
1 REPORT NUMBER 134400-7-T (Part 1)	2 GOVT ACCESSION NO	3 RECIPIENT'S CATALOG NUMBER
4 TITLE (and Subtitle) THE USE OF REMOTE SENSING IN THE DETERMINATION OF BEACH SAND PARAMETERS		5 TYPE OF REPORT & PERIOD COVERED Technical Report 3-1-78 to 2-28-79 6 PERFORMING ORG REPORT NUMBER 134400-7-T
7 AUTHOR(s) C.F. Davis, R.A. Shuchman, and G.H. Suits		8 CONTRACT OR GRANT NUMBER(s) N00014-78-C-0458
9 PERFORMING ORGANIZATION NAME AND ADDRESS Environmental Research Institute of Michigan Applications Division, P.O. Box 8618 Ann Arbor, Michigan 48107		10 PROGRAM ELEMENT PROJECT TASK AREA & WORK UNIT NUMBERS Beach Environment Task
11 CONTROLLING OFFICE NAME AND ADDRESS Geography Branch Office of Naval Research Arlington, Virginia 22217		12 REPORT DATE April 1979 13 NUMBER OF PAGES 14
14 MONITORING AGENCY NAME AND ADDRESS (if different from Controlling Office)		15 SECURITY CLASS (of this report) Unclassified 15a DECLASSIFICATION/DOWNGRADING SCHEDULE

16 DISTRIBUTION STATEMENT (of this Report)

Distribution of this document is unlimited.

17 DISTRIBUTION STATEMENT (of the abstract entered in Block 20, if different from Report)

18 SUPPLEMENTARY NOTES

This report was presented at the Thirteenth International Symposium on Remote Sensing of Environment, April 23-27, 1979. Two other papers describing this task have been submitted for publication, and will be distributed under separate cover.

19 KEY WORDS (Continue on reverse side if necessary and identify by block number)

Remote Sensing
Multispectral Scanner
Data Processing

20 ABSTRACT (Continue on reverse side if necessary and identify by block number)

A reflectance model (AQUASAND) was developed to gain insight into the spectral effects of changing mineralogy, moisture, and grain size related to beach sands. The model, a modification of the Suits radiative transfer vegetation canopy model, uses the transmittance and reflectance of the component minerals, the desired sand moisture content, and the desired sand grain size to produce a reflectance spectrum in the .35 to 2.5 μm range.

DD FORM 1 JAN 73 1473 EDITION OF 1 NOV 65 IS OBSOLETE

UNCLASSIFIED

SECURITY CLASSIFICATION OF THIS PAGE (When Data Entered)

20. ABSTRACT(continued)

Using information from AQUASAND, a mineralogy, moisture, and grain size predictive algorithms (MOGS), was developed based on laboratory sand reflectance spectra. Input to the algorithm is a set of 17 spectral reflectance "bands" simulating an airborne multispectral scanner (MSS) configuration. The MOGS algorithm first determines the appropriate mineralogical class for the input sand. Within a given class, regression equations are used to determine moisture and grain size.

The predictive results of the MOGS algorithm are very encouraging. When tested on 70 of the sand reflectance spectra from which it was derived, the correlation of actual to predicted moisture was 96%. The correlation of actual to predicted grain size based on 46 samples was 88%. Tests on independently collected sand spectra yielded similar results. The algorithm was also successfully applied to actual MSS data, collected over the Lake Michigan coastline, to generate moisture distribution and grain size distribution digital images of the beach region.

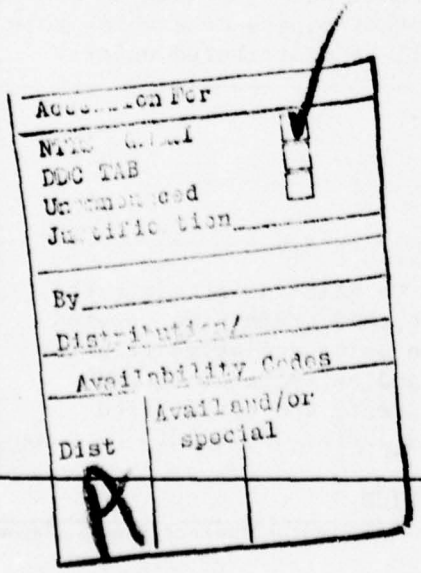

THE USE OF REMOTE SENSING IN THE DETERMINATION OF BEACH SAND PARAMETERS*

C.F. Davis, R.A. Shuchman, and G.H. Suits

Environmental Research Institute of Michigan
Ann Arbor, Michigan

ABSTRACT

A reflectance model (AQUASAND) was developed to gain insight into the spectral effects of changing mineralogy, moisture, and grain size related to beach sands. The model, a modification of the Suits radiative transfer vegetation canopy model, uses the transmittance and reflectance of the component minerals, the desired sand moisture content, and the desired sand grain size to produce a reflectance spectrum in the .35 to 2.5 μm range.

Using information from AQUASAND, a mineralogy, moisture, and grain size predictive algorithm (MOGS) was developed based on laboratory sand reflectance spectra. Input to the algorithm is a set of 17 spectral reflectance "bands" simulating an airborne multispectral scanner (MSS) configuration. The MOGS algorithm first determines the appropriate mineralogical class for the input sand. Within a given class, regression equations are used to determine moisture and grain size.

The predictive results of the MOGS algorithm are very encouraging. When tested on 70 of the sand reflectance spectra from which it was derived, the correlation of actual to predicted moisture was 96%. The correlation of actual to predicted grain size based on 46 samples was 88%. Tests on independently collected sand spectra yielded similar results. The algorithm was also successfully applied to actual MSS data, collected over the Lake Michigan coastline, to generate moisture distribution and grain size distribution digital images of the beach region.

---

1. INTRODUCTION

Historically remote sensing has been proven useful in the delineation of rock types most often with the applications of future mineral exploration in mind. In this investigation, beach sands were analyzed with the intention of determining not only mineralogy but also moisture and grain size. These three parameters are of interest from a beach trafficability and sediment transport point of view. Recognition of these parameters would also allow the identification of beach mineral deposits based on grain size and mineralogy. Since beaches are formed by intense erosion of the parent materials, harder minerals tend to be preserved and concentrated while others are dissipated. Depending on the origin of the sand, these residual minerals may be economically valuable.

In order to fully understand the effects of changes in mineralogy, moisture, and grain size on the spectral reflectance of beach sand, a sand reflectance model was used. The model, an adaptation of the Suits radiative transfer vegetation canopy model, is known as AQUASAND (Suits, 1972). It uses, as inputs,

*This work is supported by the Office of Naval Research (ONR) Contract No. N0014-74-C-0273. Mr. Hans Dolezalek is the ONR technical monitor.

the reflectance and transmittance for each mineral comprising the beach sand (i.e., quartz, feldspar, kaolinite, etc.). In addition, input to the model includes the sand grain size, the void space in the sand, and the moisture profile as a function of depth. By varying these input parameters insight was gained into the effect of physical changes on the bulk sand reflectance.

Using the information obtained from AQUASAND, the mineralogy, moisture, and grain size (MOGS) algorithm was developed using reflectance spectra measured on a Cary 14 spectrophotometer.* These spectra ranged from 0.35 to 2.5 μm, an interval practical for existing remote sensing technology. The MOGS algorithm was evaluated both on the reflectance spectra from which it was derived and on spectra collected following the algorithm development. In addition digital images of grain size distribution and moisture distribution were developed from actual multispectral scanner data.

2. PROCEDURE

The research involved in the construction of the MOGS algorithm was divided into two parts. First the Suits radiative transfer vegetation canopy model was converted to a model which could be applied to beach sands (AQUASAND) and, second, the MOGS algorithm was developed using insight obtained from the AQUASAND model.

2.1 THE AQUASAND MODEL

The most elementary model of sand reflectance is the simple plane mixture model. The model employs the assumptions that all sand particles are opaque and are randomly mixed. The surface of the sand is made up of the cross-sectional areas of the individual particles. The model calculates the bulk reflectance as being a weighted average of the particle reflectances. The model fails to achieve good accuracy because the transmittance of some particles in a finely divided state can be quite large and multiple scattering between particles is often significant.

A more complex model and the one used in this work, employs concepts identical to those employed in the directional reflectance model for vegetative canopies (Suits, 1972). Although a vegetative canopy and a sand profile are visually quite different, the essence of the reflection, transmission, and multiple scattering phenomena is much the same for both cases.

2.1.1 MODEL ASSUMPTIONS

The first assumption of the model is that the scattering components are distributed in more or less uniform layers. Because of the wind and wave action involved in the creation of a beach, sand profiles tend to be vertically stratified into horizontal layers and thus the assumption is satisfied.

The second assumption of the model is that spectral flux interacting with the sand may be divided into two types: specular and diffuse. Specular flux represents radiation which passes between the sand grains through voids and cracks without deviation. All incoming radiation is specular before it reaches the sand surface. Diffuse flux is some fraction of the specular flux which has been intercepted by a scattering component (sand grain) at least once. Following this interception it may be scattered forward or backwards, either interacting with other sand particles, or heading upwards to the sensor.

A third assumption of the model is that the individual particles making up the sand can be represented by a set of horizontal and vertical Lambertian panels which have the same reflectance and transmittance properties as do the sand particles. This assumption defines a simplified scattering phase function which allows the calculation of ensemble reflectances in closed form. Fortunately

---

*(The Cary 14 spectrophotometer is a device which is capable of digitally recording the reflectance spectrum of a surface in the .35 to 2.5 μm range.)

in sands, as in vegetative canopies, multiple scattering dominates over phase function scattering because of the high density of the scattering components. This characteristic greatly simplifies the necessary model calculations.

The fourth assumption of the model is that the diffuse flux moves in a Lambertian manner, both upward and downward, as a first approximation. The ensemble reflectance need not be perfectly Lambertian, however, it should be approximately so. Both vegetation and sand meet this criterion.

As mentioned earlier the AQUASAND model operates on the reflectance (ρ) and transmittance (τ) of a set component minerals for a given grain size to predict the reflectance spectrum of a beach. One method of obtaining the necessary ρ and τ values would be to measure them exactly for each potential grain size. This would potentially require many measurements and considerable sample preparation. Another method, and the one used in this study would be to derive the components of transmittance and reflectance for each mineral and analytically predict the ρ and τ for any given grain size. The necessary components needed to derive such information are absorption (a), internal scattering (s), and the forward scattering fraction (FS). These basic measurements were obtained by measuring the τ and ρ of 3 thin sections of each potential mineral type. Each thin section was a slightly different thickness than the others. By using an iterative curve fitting procedure the a, s, and FS values were derived using the Duntley equations (Duntley, 1942). With these values calculated at 10 nm interval throughout the spectrum we were able to predict the transmittance and reflectance spectra of a given mineral and any grain size we chose. The ρ and τ values were then entered into the AQUASAND model to produce a bulk sand reflectance spectrum (Figure 1).

Moisture content was entered into the model by adding an appropriate water spectral absorption factor at each wavelength for which a spectral value was computed for the sand. By entering the desired percent-by-volume water content the correct attenuation due to water was computed within the optical pathway equations.

2.1.2. MODEL RESULTS AND EVALUATION

By manipulating the mineralogical, grain size, and moisture model input parameters we were able to "create" any sand type we wished. Model generated spectra were compared to empirical spectra obtained from seven diverse beach types (Figure 2). The empirical measurements were made on a Cary 14 spectrophotometer which allows both continuous scanning of spectra in the .35 to 2.5 μm range and digital recording of the output spectra.

The carbonate beach type (Figure 2a) is composed of 99% exoskelatal fragments of marine organisms with approximately 1% dark organic debris mixed in. Carbonate sands are characteristically high in reflectance with high reflectance in the "red" spectral region (0.6 μm). As is apparent in Figure 2 the model captures this characteristic quite well.

Figure 2b and c are spectra of predominately iron-stained quartz beaches characteristic of the Delaware coastline. In general these spectra are depressed due to the iron staining and have substantial amounts of feldspar incorporated with them.

Figure 2d is a non-iron stained, 98% pure quartz beach. This beach type is typical of that found on the Gulf of Mexico coastline. These beaches have high reflectance due to the lack of iron stain and other dark minerals. Besides quartz there are trace amounts of carbonate and organic matter amounting to approximately 2%.

Figure 2e and f are spectra of iron-stained beaches from the Lake Michigan coastline. Both sands exhibit relatively low reflectance although spectrum 2f is definitely the lower of the two. This difference is related to the more intense iron-staining and larger percentage of opaque rock fragments in the latter beach type.

Figure 2g is a heavy mineral beach spectra collected on the coast of Oregon, which exhibits a characteristically low reflectance in the visible region. This is due to a high amount of iron-staining in addition to a large percentage of high density, opaque minerals (i.e., ilmenite, magnetite, etc.). Beaches of this type tend to have relatively low percentages of quartz, on the order of 30 to 40 percent, coupled with equal amounts of feldspar. Except for minor errors, the AQUASAND model correctly predicted the spectrum of the empirically measured sand in all seven cases. With this successful validation, work began on the algorithm predicting mineralogy, moisture, and grain size based on sand reflectance spectra in the .33 to 2.5 μm range.

2.2 DEVELOPMENT OF THE MOGS ALGORITHM

From inspection of both the AQUASAND generated, and empirical spectra it became apparent that mineralogy had by far the greatest influence on bulk reflectance. So great is this influence that it tends to mask the more subtle features of changes in grain size and, to a much lesser extent, moisture. It was decided that in order for the algorithm to handle a broad variety of sand types and still maintain the resolution needed to detect small spectral features, a preprocessing classification of mineralogy would be necessary.

2.2.1 THE CLASSIFICATION OF MINERALOGY

In order to discriminate mineralogy a vector length decision framework was used. The concept is developed as follows.

Suppose that there are two points, A and B, located in two dimensional space. The distance, or vector length, L, from A and B can be expressed in terms of the X and Y coordinate locations of points A and B as:

$$L = \sqrt{(X_A - X_B)^2 + (Y_A - Y_B)^2} \quad (1)$$

This is, of course, related to the Pythagorean Theorem. Now suppose we have a p-dimensional system with A and B located in each dimension. The vector length can be expressed as

$$L = \sqrt{\sum_{i=1}^{p} (X_{iA} - X_{iB})^2}, \quad (2)$$

where X_{iA} is the location of point A in the ith dimension and X_{iB} is the location of point B in the ith dimension.

This rationale can be used to classify some point, T, as being the member of one of n classes (A_j, j=1,n), by finding the minimum vector length from T to A_j(j=1,n). In other words T is said to be a member of the class which is closest to it, on the average, across all p dimensions. The minimum vector length is defined as

$$L_{min} = \min_{j=1,\ldots,n} \sqrt{\sum_{i=1}^{p} (X_{iT} - X_{iAj})^2} \quad (3)$$

Notice that equation 3 has no provision for variability in the n classes, therefore, L_{min} is chosen as being the shortest linear vector length. If each class has the same variability associated with it this causes no difficulty. In this experiment, however, there were considerable differences in variability between the classes so that a modification of equation 3 had to be made. The standard deviation (SD) was used to modify the distance between T and Aj related to each dimension thus removing the effects of variability from each class. This normalized minimum distance equation is expressed as

$$L_{min} = \min_{j=1,\ldots,n} \sqrt{\sum_{i=1}^{p} (X_{iT} - X_{iAj})/SD_{ij}^2}, \quad (4)$$

where SD_{ij} is the standard deviation associated with the j^{th} class in the ith dimension.

In the application of this method to the classification of mineralogy, the "dimensions" are spectral bands or ratios of spectral bands and the "classes" are mineralogical types. Eight spectral bands (Table 1) and all possible unique ratios of those spectral bands were used to classify the mineralogical type of an input sand as one of five categories (Table 2). The object was to make each category as homogeneous as possible so that the moisture and grain size regressions which followed would be sensitive to small scale spectral changes.

2.2.2. THE DEVELOPMENT OF MOISTURE AND GRAIN SIZE REGRESSIONS

Using the AQUASAND model we found that information related to moisture content of sands is best derived from the spectral region beyond 1.0 μm. This is due to the fact that the spectral reflectance of sand in this region is reduced by absorption in proportion to the amount of water present. Exceptionally high spectral absorption is noted near 1.4 and 1.9 μm. Although the spectral reflectance in these regions is highly correlated to moisture we did not consider them since atmsopheric absorption prohibits their use by an airborne sensor.

Changes in grain size seem to manifest themselves most clearly in the shorter wavelengths (.4-.7 μm). Grain size information is gained by light being reflected from sand grains below the surface through surface grains. The transmittance through the surface grains is reduced by internal scattering and absorption of the particle. Since both of these factors are dependent on thickness, the bulk reflectance of a sand is dependent to some degree on the grain size. Theoretically a large grain sand should have a lower reflectance than a small grain sand of the same mineralogical composition and with similar moisture content. According to our measurements this appears to be the case.

This grain size phenomenon can be confounded in two ways. First if there is no scattering or absorption within the grains (i.e., a perfectly clear material at all wavelengths) there can be no attenuation. Fortunately, even in our purest quartz sands there were enough impurities and inclusions to give some attenuation. Second, the sand grains may be opaque and thus attenuate too much light. This appears to be the case in the heavy mineral and carbonate beaches. Most of the bulk reflectance for these two types was due to surface reflectance and little if any was due to light transmitted through the surface grains from below. We were unable to create accurate grain size equations for these types.

Utilizing the physical phenomena discussed above we were able to develop multiple linear regression equations for predicting moisture in all five mineralogical classes and grain size for three of the five mineralogical classes. The basis for all the regressions except one was the sample group corresponding to a given mineralogical class. The single exception was the grain size equation corresponding to a pure quartz beach. Our samples within this type consisted of a single grain size (0.22 mm) and, as such did not provide an adequate basis for regression equations. For this case we used AQUASAND generated spectra to simulate a wide range of grain sizes in order to add grain size variability to the data set.

Seventeen spectral bands between 0.4 and 2.5 μm were chosen for use in the regressions (Table 3). Within the 17 bands, only those which were predicted by the AQUASAND model to be most informative were used. In this way we could be reasonably certain that the regression equations would respond the correct parameter and thus yield accurate predictions. The predictive equations together with the associated standard errors (SE), and coefficient of variation (R^2) are given in Table 4.

In summary the MOGS algorithm (Figure 3) represents a computer controlled package of equations. The input is a set of 17 spectral reflectance bands obtained from an unknown sand. Based on these bands, the sand is classified as being a member one of five mineralogical types. Depending on the mineralogical type, the appropriate moisture and grain size (where applicable) equations are applied to the data. The output from the MOGS algorithm is the predicted mineralogical class, the predicted moisture, and the predicted grain size.

3. TEST RESULTS OF THE MOGS ALGORITHM ON LABORATORY SPECTRA

The MOGS algorithm was first tested on 70 of the 81 samples from which it was derived and the results were very promising as can be seen in Table 5. The classification of mineralogy was 99+% correct. The overall correlation of predicted to actual moisture was 96% (significant at the .001 level) and the overall correlation of predicted to actual grain size was 88% (significant at the .001 level). However, testing any equation or algorithm on the samples from which it was derived is not conclusive. For this reason the MOGS algorithm was tested on several other beach sand samples which were independently collected and spectrally measured following the algorithm construction. These results are given in Table 6. In each case the MOGS algorithm selected a mineralogy which allowed the moisture and grain size regression to operate correctly. The independent test yielded an actual moisture to predicted moisture correlation of .95 (significant at the .01 level). The prediction of grain size was in no case more than 0.07 mm different from the actual grain size.

4. TEST OF THE MOGS ALGORITHMS ON MSS DATA

The next logical test for the MOGS algorithm was to evaluate it on actual MSS data. Such an investigation is presently underway using data obtained from the Environmental Research Institute of Michigan (ERIM) multispectral-scanner (MSS) flown over a portion of the Lake Michigan shoreline (November 1, 1978). The MOGS algorithm was modified to conform to the 12 band configuration of the ERIM scanner.

Although a complete discussion of the Lake Michigan MSS test is beyond the scope of this paper, preliminary results look quite good (Table 7). The correlation of predicted to actual moisture content is .91 (significant at the .01 level) and the prediction of grain size is, in no case, greater than .09 mm different from the actual grain size.

The moisture prediction appears particularly poor for high moisture contents. This may be due to the fact that wet sand at the test sites appeared to exhibit bi-directional dependencies (i.e., a failure to behave in a Lambertian manner). These bi-directional characteristics are enhanced at low sun angles and are not accounted for by the MOGS algorithm. Although the flight took place at 1:30 EST the sun was only 38° above the horizon on November 1. To minimize bi-directional reflectance, future aircraft flights should be made during complete mid-altitude (3000 m) cloud cover or sunny skies with the sun close to the zenith (summer sun).

Applying the same moisture and grain size equations used in the previous analysis, the entire Pentwater State Park beach on a pixel by pixel basis (in this case 1.5 x 1.5 meters) was classified with respect to grain size and moisture content. The two MOGS generated digital maps (see Figure 4) show the predicted moisture and grain size distributions on the beach at Pentwater. The ground truth measurements taken at the time of flight correlate well with these images. Figure 4 helps to demonstrate how an entire sandy coastline could be analyzed in respect to moisture, grain size, and gross mineralogy using a small subsection as calibration.

5. CONCLUSION

The development of the MOGS algorithm has demonstrated the feasibility of obtaining quantitative moisture and grain size information from the spectral reflectance of beach sands. The determination of grain size is dependent on the sand grains being neither opaque or perfectly clear.

The two stage nature of the MOGS algorithm is directly responsible for its broad applicability without loss of detail. By separating the mineralogical types prior to the prediction of moisture and grain size much of the variability which could easily hide small scale changes is removed. The use of a vector length discriminant function to classify mineralogy worked extremely well in this application, since 36 different dimensions could be simultaneously evaluated. The use of a multistage approach involving multiple classification

techniques is a powerful tool; one which will very likely be useful in many areas of remote sensing.

The Lake Michigan field test has further demonstrated the MOGS algorithm's applicability to actual remotely sensed data. Grain size was predicted to within .09 mean diameter of actual while beach moistures less than 2% were accurately predicted. In all cases the computer algorithm correctly identified the Michigan beach mineralogy as being a predominantly quartz iron stained-feldspar beach.

Table 1. The 8 spectral bands used in the breakdown of beach mineralogy into 1 of 5 categories. In addition to these 8 bands all unique ratio combinations were also used.

Band #	Wavelength Range (μm)
1	.43-.47
2	.47-.49
3	.51-.53
4	.53-.56
5	.59-.63
6	.80-.90
7	.90-1.0
8	1.0-1.1

Table 2. The 5 potential mineralogical classifications

Class #	Description
1	Iron stained Atlantic coast type
2	Iron stained Michigan coast type
3	Iron stained pure quartz type
4	Heavy mineral type
5	Carbonate type

Table 3. The 17 bands used in the development of moisture and grain size regression equations

Band #	Wavelength Range (μm)
1	0.43-0.47
2	0.47-0.49
3	0.49-0.51
4	0.51-0.53
5	0.53-0.56
6	0.56-0.59
7	0.59-0.63
8	0.63-0.67
9	0.70-0.75
10	0.75-0.80
11	0.80-0.90
12	0.90-1.00
13	1.00-1.10
14	1.10-1.20
15	1.20-1.35
16	1.50-1.85
17	2.10-2.50

Table 4. Multiple linear regression equations for the prediction of moisture and grain size. The equations are listed by mineralogical class. Grain size is in mm.

a. Iron stained quartz - Atlantic coast

Predicted moisture % = $67.964 - 65.046 \left(\frac{\text{Band 16}}{\text{Band 14}}\right)$

S.E. = 3.08%, $R^2 = 0.888$

Predicted grain size = $6.87 - 3.4634 (\text{Band 7})^{1/4} + .0300 (\text{Band 1}) + .01672 (\text{Band 15})$

S.E. = 0.13 mm, $R^2 = 0.603$

b. Iron stained quartz - Michigan coast

Predicted moisture % = $60.149 - 49.961 \left(\frac{\text{Band 16}}{\text{Band 11}}\right) - 2.226 \left(\frac{\text{Band 17}}{\text{Band 1}}\right)$

S.E. = 2.56%, $R^2 = .970$

Predicted grain size = $0.6405 - 0.0152 (\text{Band 5}) - .0047 (\text{Band 17})$

S.E. = 0.055 m, $R^2 = 0.558$

c. Non-Iron stained quartz

Predicted Moisture % = $127.02 - 65.159 \left(\frac{\text{Band 16}}{\text{Band 15}}\right) - 64.054 \left(\frac{\text{Band 15}}{\text{Band 14}}\right)$

S.E. = 2.12%, $R^2 = 0.971$

Predicted grain size = $1.158 - 2.328 (\text{Band 10}) + .3201 \left(\frac{\text{Band 7}}{\text{Band 1}}\right) + 0.2858 (\text{Band 16})$

S.E. and R^2 not applicable

d. Carbonate

Predicted moisture % = $596.28 - 642 \left(\frac{\text{Band 14}}{\text{Band 17}}\right) - 1.081 (\text{Band 14}) + 0.1538 (\text{Band 17})$

S.E. = 4.09%, $R^2 = .879$ No grain size equation.

e. Heavy mineral

Predicted Moisture % = $19.284 + 11.194 \left(\frac{\text{Band 14}}{\text{Band 17}}\right) - 1.081 (\text{Band 14}) + 0.1538 (\text{Band 17})$

S.E. = 4.09%, $R^2 = .879$ No grain size equation.

Table 5. Comparison of actual sand parameters to predicted classification by the MOGS algorithm

Sand I.D.		Moisture %		Grain Size mn	
Actual	Predicted	Actual	Predicted	Actual	Predicted
A1	A	4.5	3.8	.35	.36
A2	A	29.4	26.4	.35	.46
A3	A	15.0	11.8	.37	.40
A4	A	28.4	28.0	.50	.48
A5	A	11.3	12.9	.43	.49
A6	A	33.4	27.1	.32	.39
A7	A	13.1	13.8	.35	.43
A8	A	24.9	27.3	.38	.37
A9	A	8.8	19.4	.44	.30
A10	A	29.7	27.9	.43	.44
B1	B	21.0	17.8	.40	.62
B2	B	24.6	25.5	.76	.58
B3	B	14.2	15.1	.46	.57
B4	B	27.2	26.3	.88	.76
B5	B	11.0	8.9	.63	.82
B6	B	19.0	25.6	.95	.76
B7	B	26.8	28.2	.71	.76
B8	B	24.9	21.0	.76	.63
B9	B	6.2	5.9	.71	.62
B10	B	*	7.5	.71	.57
B11	B	20.0	23.0	.81	.76
B12	B	34.0	33.1	.69	.73
B13	A	6.0	4.4	.55	.60
B14	B	31.0	26.0	.83	.71
B15	B	18.0	22.2	.67	.69
B16	B	32.0	31.5	.57	.72
B17	B	18.0	20.8	.56	.67
B18	B	23.0	23.9	.65	.76
B19	B	3.0	7.1	.94	.68
B20	B	23.0	27.8	.60	.61
M1	M	5	8.2	.36	.27
M2	M	15	13.4	.36	.28
M3	M	25	26.2	.36	.34
M4	M	30	27.4	.36	.36
M5	M	5	5.5	.41	.38
M6	M	15	15.7	.41	.45
M7	M	0	0.0	.23	.31
M8	M	0	0.0	.29	.29
M9	M	0	0.0	.41	.39
M10	M	0	0.0	.36	.35
M11	M	10	12.0	.23	.31
M12	M	25	24.4	.23	.28
M13	M	30	27.2	.23	.25
M14	M	10	12.8	.41	.36
M15	M	20	20.6	.41	.40
M16	M	15	16.8	.23	.26
01	H	0	0	no grain size	
02	H	5	6.4	no grain size	
03	H	10	11.7	no grain size	
04	H	15	20.3	no grain size	
05	H	20	22.0	no grain size	
06	H	25	21.9	no grain size	
07	H	30	27.5	no grain size	

*No moisture data

Table 5. (Continued)

Sand I.D.		Moisture %		Grain Size mn	
Actual	Predicted	Actual	Predicted	Actual	Predicted
08	H	35	24.7	no grain size	
MX1	MX	25	24.6	.22	.32
MX2	MX	0	0.0	.22	.10
MX3	MX	10	14.1	.22	.13
MX4	MX	15	18.1	.22	.22
MX5	MX	30	34.2	.22	.4
MX6	MX	35	33.7	.22	.34
MX7	MX	20	23.1	.22	.33
MX8	MX	5	6.9	.22	.11
C1	C	0	0	no grain size	
C2	C	10	7.8	no grain size	
C3	C	5	5.7	no grain size	
C4	C	20	13.4	no grain size	
C5	C	15	18.8	no grain size	
C6	C	30	30.8	no grain size	
C7	C	25	27.9	no grain size	
C8	C	40	38.4	no grain size	
C9	C	50	46.4	no grain size	

Table 6. Comparison of actual parameters to predicted classificattions by the MOGS algorithm. Samples used here were collected independently of those on which the algorithm is based.

Sample Mineralogy		Moisture %		Grain Size (mm)	
Actual	Predicted	Actual	Predicted	Actual	Predicted
MICH1	MICH	37.7	25.6	.26	.28
MICH2	MICH	3.2	3.7	.28	.30
MICH3	MICH	0.3	0.0	.25	.32
MICH4	MICH	12.1	16.0	.23	.29
MICH5	MICH	15.0	12.7	.25	.30
MICH6	MICH	28.0	26.2	.28	.29

Table 7. Comparison of actual parameters to predicted classifications by the MOGS algorithm. The sand spectra used here were collected by the ERIM MSS.

Sample Mineralogy		Moisture %		Grain Size (mm)	
Actual	Predicted	Actual	Predicted	Actual	Predicted
MICH1	MICH	22.3	12.1	.25	.32
MICH2	MICH	1.0	0.0	.23	.28
MICH3	MICH	8.0	10.1	.22	.25
MICH4	MICH	28.0	16.9	.26	.35
MICH5	MICH	5.0	2.2	.24	.26

LITERATURE CITED

Duntley, S.Q. 1942. The Optical Properties of Diffusing Materials, Journ. Amer. Opt. Soc. Vol. 32, p. 61-69.

Suits, G.H. 1972. The Calculation of the Directional Reflectance of a Vegetation Canopy. Rem. Sens. of Env. Vol. 2, pp. 117-125.

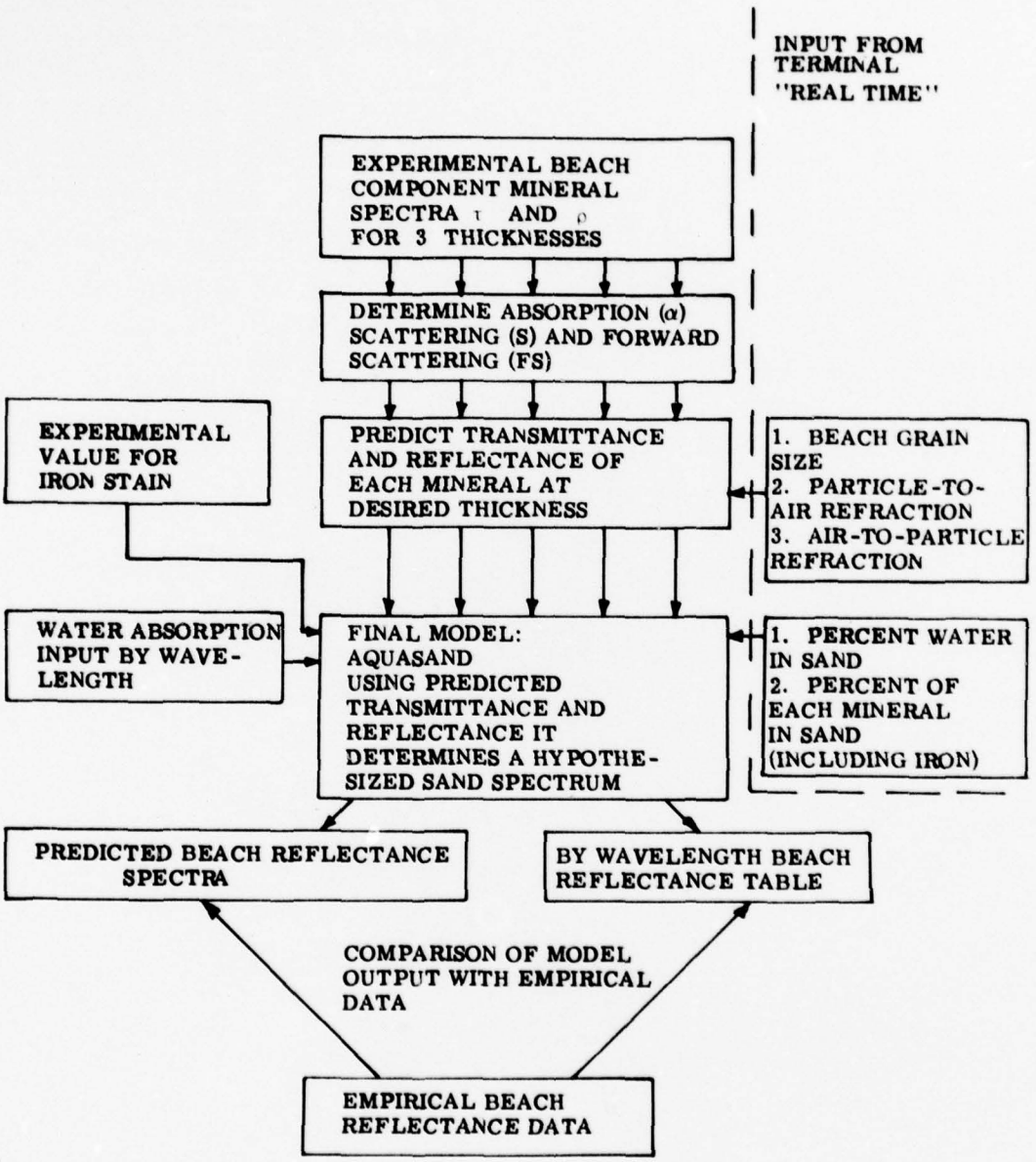

Figure 1. Flow diagram of the AQUASAND MODEL.

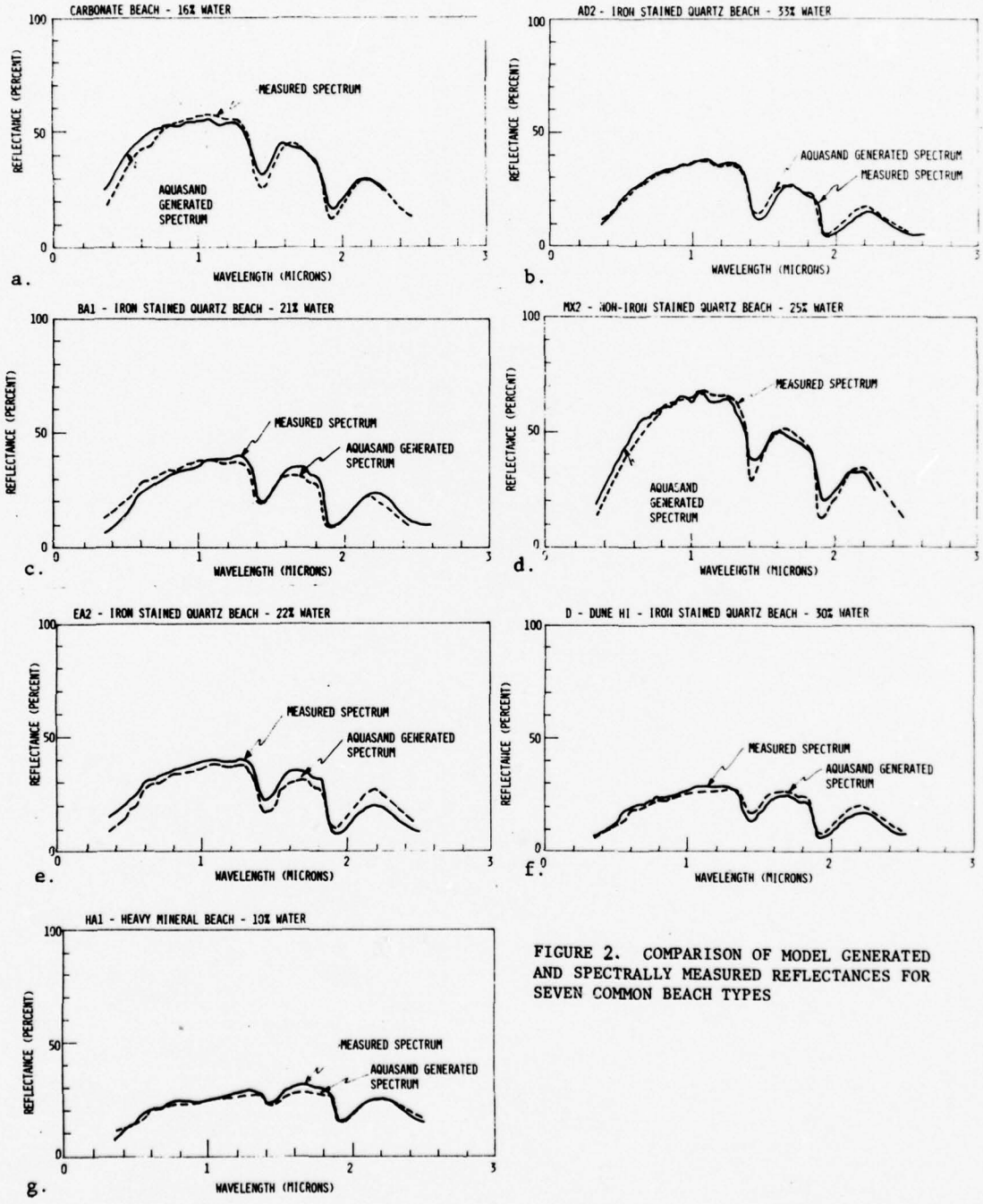

FIGURE 2. COMPARISON OF MODEL GENERATED AND SPECTRALLY MEASURED REFLECTANCES FOR SEVEN COMMON BEACH TYPES

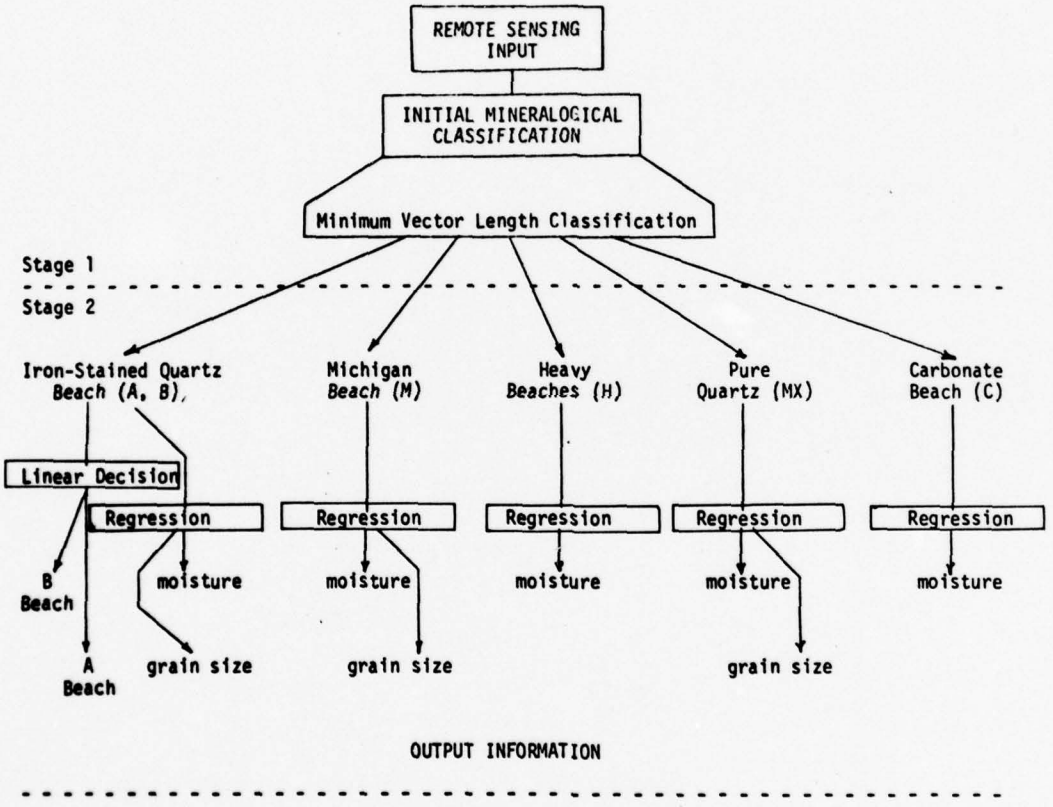

FIGURE 3. FLOW DIAGRAM OF THE MOGS ALGORITHM.

MOISTURE DISTRIBUTION IMAGE - LIGHTER SHADE INDICATES HIGHER MOISTURE CONTENT

0-5% 5-20% 20+%

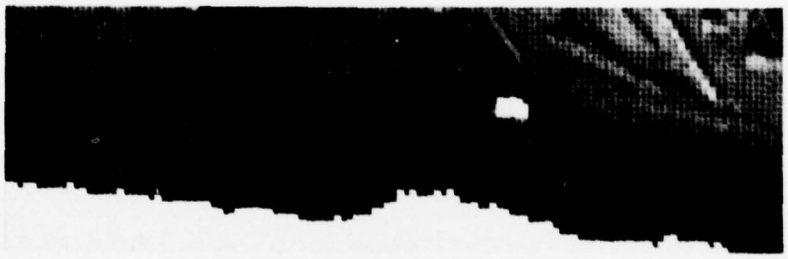

GRAIN SIZE DISTRIBUTION IMAGE - LIGHTER SHADE INDICATES LARGER GRAIN SIZE

.15-.25 mm .25-.40 mm >.40 mm

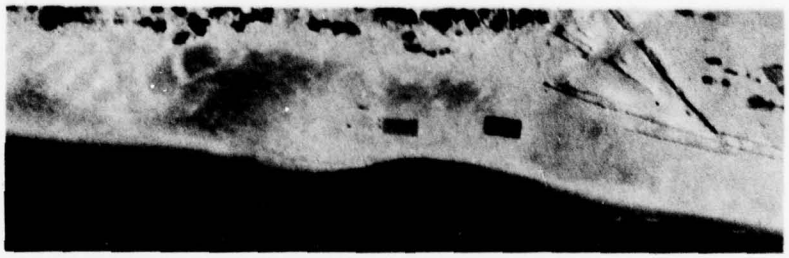

PANCHROMATIC AERIAL PHOTOGRAPH

RE 4. DIGITAL IMAGERY, GENERATED BY THE MOGS ALGORITHM SHOWING THE DISTRIBUTION OF MOISTURE AND GRAIN SIZE ON PENTWATER BEACH (PENTWATER STATE PARK, MICHIGAN). WHITE AREAS ARE EITHER UNCLASSIFIED REGIONS OR OPEN WATER.

UNCLASSIFIED

SECURITY CLASSIFICATION OF THIS PAGE (When Data Entered)

REPORT DOCUMENTATION PAGE		READ INSTRUCTIONS BEFORE COMPLETING FORM
1 REPORT NUMBER 134400-7-T (Part 2)	2 GOVT ACCESSION NO	3 RECIPIENT'S CATALOG NUMBER
4 TITLE (and Subtitle) SHALLOW WATER REFLECTANCE MODELING WITH APPLICATIONS TO REMOTE SENSING OF THE OCEAN FLOOR		5 TYPE OF REPORT & PERIOD COVERED TECHNICAL REPORT 3/1/78 to 2/28/79 6 PERFORMING ORG REPORT NUMBER 134400-7-T
7 AUTHOR(s) D. R. Lyzenga		8 CONTRACT OR GRANT NUMBER(s) N00014-78-C-0458
9 PERFORMING ORGANIZATION NAME AND ADDRESS Environmental Research Institute of Michigan P.O. Box 8618, APPLICATIONS DIVISION Ann Arbor, MI 48107		10 PROGRAM ELEMENT, PROJECT, TASK AREA & WORK UNIT NUMBERS Marine Environment Task
11 CONTROLLING OFFICE NAME AND ADDRESS Geography Branch Office of Naval Research Arlington, VA 22217		12 REPORT DATE April 1979 13 NUMBER OF PAGES 20
14 MONITORING AGENCY NAME AND ADDRESS (if different from Controlling Office)		15 SECURITY CLASS (of this report) Unclassified 15a DECLASSIFICATION/DOWNGRADING SCHEDULE

16 DISTRIBUTION STATEMENT (of this Report)

Distribution of this document is unlimited.

17 DISTRIBUTION STATEMENT (of the abstract entered in Block 20, if different from Report)

18 SUPPLEMENTARY NOTES

This report was presented at the Thirteenth International Symposium on Remote Sensing of Environment, April 23-27, 1979.

19 KEY WORDS (Continue on reverse side if necessary and identify by block number)

REMOTE SENSING
MULTISPECTRAL SCANNER
DATA PROCESSING

20 ABSTRACT (Continue on reverse side if necessary and identify by block number)

Features attributable to the reflection of light from the ocean floor are observable in remote sensing data for water depths less than 1-2 optical attenuation lengths. Information about the characteristics of the bottom and the water depth can be obtained by comparing the observed radiances in two or more wavelength bands with radiances calculated from a radiative transfer model.

DD FORM 1 JAN 73 1473 EDITION OF 1 NOV 65 IS OBSOLETE

UNCLASSIFIED

SECURITY CLASSIFICATION OF THIS PAGE (When Data Entered)

20. ABSTRACT (Continued)

To first order, the bottom-reflected radiance in a given spectral band is proportional to the bottom reflectance and exponentially dependent on the water depth. Deviations form this simple model are caused by volume scattering, internal reflection at the water surface, and effects due to the variation of water parameters within the spectral bandwidth of the detector. Most of these effects are not readily observable in remote sensing data because of the spatial variability of water and bottom parameters. Thus, the simple model is useful for understanding the main features of the data and for suggesting methods of extracting the desired information from the scanner data, but a more comprehensive radiative transfer model is needed to evaluate the accuracy of these methods.

As an example of the application of radiative transfer models, an algoritiim for mapping bottom reflectance variations is described, and an evaluation of this algorithm is presented using a model based on the quasi-single-scattering approximation. Input parameters for this model include water attenution coefficients tabulated by Jerlov, volume scattering functions reported by Petzold, and bottom reflectances measured in St. Andrew Bay, Florida. Results are presented for the case of clear ocean water (Jerlov type 1B) and for relatively turbid coastal water (Jerlov type 5). The effects of system noise are included, and the improvement in classification accuracy obtained by increasing the number of input wavelength bands is evaluated.

SHALLOW-WATER REFLECTANCE MODELING WITH APPLICATIONS TO REMOTE SENSING OF THE OCEAN FLOOR

David R. Lyzenga

Environmental Research Institute of Michigan
Ann Arbor, Michigan

ABSTRACT

Features attributable to the reflection of light from the ocean floor are observable in remote sensing data for water depths less than 1-2 optical attenuation lengths. Information about the characteristics of the bottom and the water depth can be obtained by comparing the observed radiances in two or more wavelength bands with radiances calculated from a radiative transfer model.

To first order, the bottom-reflected radiance in a given spectral band is proportional to the bottom reflectance and exponentially dependent on the water depth. Deviations from this simple model are caused by volume scattering, internal reflection at the water surface, and effects due to the variation of water parameters within the spectral bandwidth of the detector. Most of these effects are not readily observable in remote sensing data because of the spatial variability of water and bottom parameters. Thus, the simple model is useful for understanding the main features of the data and for suggesting methods of extracting the desired information from the scanner data, but a more comprehensive radiative transfer model is needed to evaluate the accuracy of these methods.

An an example of the application of radiative transfer models, an algorithm for mapping bottom reflectance variations is described, and an evaluation of this algorithm is presented using a model based on the quasi-single-scattering approximation. Input parameters for this model include water attenuation coefficients tabulated by Jerlov, volume scattering functions reported by Petzold, and bottom reflectances measured in St. Andrew Bay, Florida. Results are presented for the case of clear ocean water (Jerlov type IB) and for relatively turbid coastal water (Jerlov type 5). The effects of system noise are included, and the improvement in classification accuracy obtained by increasing the number of input wavelength bands is evaluated.

1. INTRODUCTION

Remote sensing data over shallow water areas contain information about both the water depth and the bottom composition, since both of these factors contribute to the observed radiance. The feasibility of extracting this information depends on the extent to which the contributions of each of these factors can be separated. The role of modeling is to determine the dependence of the observed radiance upon all of the relevant physical factors, to devise methods or algorithms for extracting information about these factors from the observed radiance, and to evaluate the accuracy of these algorithms under various conditions.

In this paper, efforts at modeling the reflectance of shallow water are described and an example of the use of these models for devising and evaluating

information extraction algorithms is presented. The example is of an algorithm for recognizing and classifying bottom types under a variable depth of water. This problem is in a sense prior to the problem of calculating water depths from multispectral scanner data, since bottom types can be recognized without knowledge of the water depth but the water depth cannot be calculated in the general case without knowledge of the bottom type.* In addition to its relevance to the problem of remote sensing of water depth, the capability of mapping bottom reflectance variations may be useful in geological and biological studies of the shallow ocean floor. Reflectance variations are caused mainly by the growth of benthic vegetation, which is indicative of the substrate material and of ecological conditions in the littoral zone. Muds and silts can also be discriminated from quartz or carbonate sand as another indication of bottom conditions.

2. SHALLOW-WATER REFLECTANCE MODELS

The reflectance of the ocean or of any other body of water is determined by the surface state, the optical properties of the water, and in the case of shallow water by the depth and reflectance of the bottom. Since the water reflectance cannot be calculated exactly, except by numerical methods, a number of approximate models have been developed. Some of these models are described in the following sections.

2.1 SIMPLE ATTENUATION LAW

It is well known that in an absorbing medium the intensity of radiation decreases exponentially with distance (Bouguer's Law). Although this law holds strictly for collimated light, or light measured with a detector having a narrow field of view, the assumption is commonly made that the same law holds for irradiance. Thus, measurements of downwelling irradiance in the ocean are summarized by the irradiance attenuation coefficient**, K, which implies that the irradiance decreases with depth according to the equation.

$$E(z) = E(o)\ e^{-Kz} \tag{1}$$

The simplest model for predicting the reflectance of a shallow body of water is to assume that this relationship holds for both downwelling light and upwelling light reflected from the bottom. Thus, for a water depth z and a bottom reflectance R_b, the reflectance of the body of water is given by the simple equation

$$R = kR_b\ e^{-2Kz} + R_s \tag{2}$$

where k is a factor which includes the transmittance of the water surface for downwelling and upwelling light, and R_s is the reflectance of the water surface. When the reflectance is measured from an aerial platform, the same formula is used except the factor k must include the transmittance of the atmosphere and R_s must include the path radiance.

Despite the crudeness of this model, it seems to account quite well for the signals recorded by a multispectral scanner over shallow water. Deviations certainly occur from the purely exponential dependence on depth predicted by the model, but the variability in bottom reflectance and water attenuation coefficients in most natural areas provides a plausible explanation for these deviations.

---

*In many cases the depth can be calculated to a good approximation without exact knowledge of the bottom type by assuming that the ratio of the bottom reflectances in two wavelength bands is the same for all bottom types in the scene.

**Also called the diffuse attenuation coefficient, although this term is misleading since it implies that the direct beam is excluded from the measurement, whereas the measurement actually includes both direct and diffuse irradiance.

Experimentally then, this model has not been conclusively disproved with remote sensing data. Theoretically, however, these are reasons for mistrusting this simple model and there are methods of constructing more accurate models based upon the radiative transfer equation. Some of these models are discussed in the following section.

2.2 RADIATIVE TRANSFER MODELS

The radiative transfer equation in principle completely describes the radiation field in any macroscopic medium in terms of the scattering function and the optical depth within the medium. Since this equation does not have exact analytical solutions, except in the simplest cases, two approaches may be taken to obtain useable results. One approach is to apply numerical integration techniques to solve the equation for a specific set of conditions. Examples of this approach are matrix operator methods [1] and Monte Carlo methods [2]. Given enough computer time these methods can yield results to any required degree of accuracy, but because of the highly anisotropic nature of the scattering function in water some compromises with accuracy must usually be made to keep the time and cost within acceptable limits.

The other approach to using the radiative transfer equation is to obtain approximate analytical solutions by simplifying either the equations or the form of the scattering function. In the two-stream approximation [3] the radiation field is characterized by two parameters and a simplified form of the transfer equation is assumed. Neglecting the effects of internal reflection at the water surface, this approximation yields the following equation for the subsurface reflectance of a shallow body of water:

$$R'_w = \frac{R_b\sqrt{1-x^2}\cosh(Kz) + (x-R_b)\sinh(Kz)}{\sqrt{1-x^2}\cosh(Kz) + (1-xR_b)\sinh(Kz)} \tag{3}$$

where $$x = \frac{b}{a+b} \tag{4}$$

and $$K = \sqrt{a^2 + 2ab} \tag{5}$$

a is the absorption coefficient and b is the backscattering coefficient of the water. A plot of this reflectance as a function of Kz is shown in Figure 1 for the case $R_b = 0.5$, with values of x ranging from 0.1 to 0.9. As $z \to \infty$, the subsurface reflectance approaches the value

$$R'_v = \frac{x}{1+\sqrt{1-x^2}} \tag{6}$$

The reflectance predicted by this model can be closely approximated by the equation

$$R'_w = R'_b\, e^{-2Kz} + R'_v \tag{7}$$

where

$$R'_b = R_b - R'_v \tag{8}$$

and K is defined by equation (5). The difference between equations (3) and (7) is less than 2 percent for $R_b \leq 0.5$. Thus, the effects of scattering as calculated by this model can be described in terms of the simple attenuation law as a decrease in the apparent bottom reflectance and an increase in the deep-water reflectance. This model does not allow the angular distribution of the light to be calculated, nor does it account for changes in the angular distribution of the light field with depth. Thus, it does not allow a complete assessment

of the effects of scattering in the water, but it does demonstrate that back-scattering per se does not cause a noticeable deviation from the exponential dependence on depth predicted by the simple attenuation model.

Another approximate solution of the radiative transfer equation is the quasi-single-scattering approximation [4]. In this approximation the actual scattering function, which is strongly peaked at $\theta=0$, is replaced by the function

$$p'(\theta) = \begin{cases} \frac{F}{2\pi}\,\delta(\theta), & \theta < \frac{\pi}{2} \\ p(\theta), & \theta \geq \frac{\pi}{2} \end{cases} \tag{9}$$

and the effects of multiple scattering are neglected by dropping the integral term in the radiative transfer equation. The angular distribution of the upwelling light can be calculated with this approximation, although the angular distribution of the downwelling light is not accurately represented, since all forward scattering is assumed to be concentrated in a single direction. For direct incident light, the radiance predicted by the quasi-single-scattering approximation can again be written as a simple exponential function of the depth. In this case, the deep-water radiance beneath the surface is given by

$$L'_v = \frac{\beta(\mu_s)\, E'_o}{(a+b)\,(\mu+\mu_o)} \tag{10}$$

where E'_o is the downwelling irradiance beneath the surface, μ_o is the cosine of the angle of incidence (under water), μ is the cosine of the view angle under water, μ_s is the cosine of the angle between these two directions, and $\beta(\mu_s)$ is the volume scattering function for the water. The attenuation coefficient is given by

$$K_d = (a+b)/\mu_o \tag{11}$$

for the downwelling irradiance and

$$K_u = (a+b)/\mu \tag{12}$$

for the upwelling radiance. The diffuse reflectance can be obtained from this model by integrating over μ and μ_o. This gives rise to a slightly non-exponential behavior since the radiance at larger polar angles is attenuated more rapidly than that at small angles.

A second effect which causes a deviation from the simple attenuation law is the effect of internal reflection at the water surface. Although only a small fraction of the upwelling light is reflected from the water surface at normal incidence, this fraction increases to 100 percent at the critical angle (48.6°). If the upwelling light is isotropically distributed, the total fraction of the upwelling irradiance reflected at the surface is about 48 percent. The effects of internal reflection can be incorporated into the radiative transfer equation as a boundary condition, and evaluated exactly using numerical methods. An approximate evaluation of this effect can also be made by assuming that beneath the surface the body of water acts as a Lambertian reflector. The total reflectance above the surface is then

$$R = \frac{(1-R_s)(1-R'_s)R'_w}{1-R'_sR'_w} + R_s \tag{13}$$

where R'_w is the subsurface reflectance, R'_s is the internal reflectance of the water surface (0.475), and R_s is the external reflectance of the water surface (0.020 for collimated light incident normally, 0.067 for diffuse light). This effect is illustrated in Figure 2 for various values of the bottom reflectance. The dashed lines in this figure indicate the reflectance calculated from the simple attenuation law ignoring internal reflection effects and the solid lines indicate the reflectance calculated from equation (13). The effect of internal reflection is appreciable for very shallow water and high bottom reflectances, but falls off rapidly with increasing water depth.

A third effect which causes a deviation from a purely exponential relationship between the reflectance and the water depth is the effect of averaging the reflectance over a range of wavelengths. The previous equations for reflectance are strictly true only for monochromatic light. When light is collected by a detector system having a finite spectral bandwidth, the spectral components within this bandwidth may be attenuated at different rates. As a result the total irradiance within the band has a larger effective attenuation coefficient in shallow water where all components are present than in deeper water where only the less rapidly attenuated components remain. An example of this effect is shown in Figure 3. This figure shows the reflectance for Jerlov's water type IB with a sand bottom, calculated from a model based on the quasi-single-scattering approximation including the effects of internal reflection. The dashed lines indicate the monochromatic reflectances at 0.55 μm and 0.65 μm as a function of water depth. The solid lines indicate reflectances averaged over Landsat bands MSS4 and MSS5, which are centered at the same wavelengths but have bandwidths of 0.10 μm each. The effective attenuation coefficient for MSS4, as indicated by the slope of the upper solid line, is slightly larger than the attenuation coefficient at 0.55 μm in shallow water, but approaches the same value in deeper water. In the case of MSS5, the effective attenuation coefficient is equal to the monochromatic value in shallow water but becomes smaller as the depth increases. The magnitude of this effect depends upon the degree to which the attenuation coefficient varies over the spectral band under consideration. Thus, if the band is narrow or is located in a region of the spectrum where the attenuation coefficient is relatively constant, the effect may be negligible. For broadband systems, however, the effect is appreciable.

2.3 INPUT PARAMETERS FOR WATER REFLECTANCE MODELS

A complete set of input parameters for calculating the shallow water reflectance would include the spectral absorption and scattering coefficients of the water, the volume scattering function, and the bottom reflectance. Unfortunately, simultaneous measurements of all these parameters are very scarce. Petzold [5] has measured volume scattering functions at one wavelength for several different water types (Figure 4) and used the measurements along with the beam attenuation coefficient to infer the absorption and scattering coefficients. However, spectral measurements of these quantities are still lacking. Jerlov [6] has devised a scheme of optical classification of water types, and tabulated spectral values of the irradiance attenuation coefficient for each type (Figure 5). No information is given by Jerlov about the scattering properties of these water types.

In order to synthesize these measurements into a complete set of optical properties, the empirical relationship reported by Shannon [7] between beam attenuation coefficients and irradiance attenuation coefficients has been used to estimate the scattering coefficient for each of Jerlov's water types. An average scattering function was obtained from Petzold's measurements by summing the volume scattering functions for all the stations and dividing by the sum of the scattering coefficients. The wavelength dependence of the scattering function is estimated by decomposing the scattering function into a Rayleigh or molecular component and a particulate component. The Rayleigh component varies with the fourth power of the wavelength, and the particle component is assumed to be wavelength independent.

Measurements of bottom reflectance are even more scarce than water optical properties. A limited number of bottom reflectance measurements were made by the author in St. Andrew Bay, Florida using an ISCO Spectroradiometer with a

submersible fiber optic probe. The radiance just above the bottom was measured and compared with the radiance over a set of calibrated reflectance panels on the bottom. This method allows corrections to be made for absorption and scattering in the water path between the detector and the bottom. The results of these measurements for sand, shoal grass, and turtle grass are shown in Figure 6. Other sources of information include measurements made using a photographic technique with filters and reflectance panels for a variety of bottom types in the Bahamas [8]*, and laboratory measurements of beach sands from a number of locations using a Cary-14 spectrometer [9].

3. BOTTOM RECOGNITION ALGORITHM

The problem of mapping bottom reflectance variations under a variable depth of water is illustrated in Figure 7. This figure shows a portion of Landsat frame 1925-15015 over the Great Bahama Bank. A comparison with hydrographic charts of the area shows a general correlation between the MSS4 reflectance and the water depth, but there are some notable discrepancies. The two areas indicated on the image have the same MSS4 signal level (about 28 digital counts), but the lower area has a depth of 3 meters while the upper area is about twice as deep. Low-altitude color aerial photography shows that the lower area is quite heavily vegetated, presumably because of the protection afforded by the row of islands to the west, while the upper area has a sand bottom. Thus, the difference in depth is offset by the change in bottom reflectance, causing the MSS4 signal to be the same in both areas. In order to separate the effects of water depth and bottom reflectance, an algorithm which combines information from at least two wavelength bands is needed. Conventional multispectral classification techniques do not work well for this purpose because they depend upon the existence of well-defined spectral signatures for each category, which do not exist in this case because of the effects of water depth variations. An algorithm which combines the signals in such a way as to remove the effects of water depth variations is described in the following section.

3.1 FORMULATION OF ALGORITHM

A method of combining multispectral signals in order to create a depth-invariant index of the bottom type is suggested by the simple reflectance model described in section 2.1. This model predicts that if the radiances over a given bottom type are plotted in the space defined by the variables

$$X_i = \ln(L_i - L_{si}) \tag{14}$$

where L_i is the radiance in band i for water depth z and L_{si} is the deep-water radiance, the set of points generated by allowing z to vary continuously over a range of depths will fall along a straight line having direction cosines

$$\gamma_i = K_i / \sqrt{\sum_{j=1}^{n} K_j^2} \tag{15}$$

which are independent of the bottom reflectance. For a different bottom type, the radiances will, therefore, fall along a parallel line which is displaced from the first by a distance

$$d^2 = \sum_{i=1}^{n} (\ln r_{bi})^2 - \left(\sum_{i=1}^{n} \gamma_i \ln r_{bi}^2\right) \tag{16}$$

where r_{bi} is the ratio of bottom reflectances** for the two bottom types in

---

*Further measurements of bottom reflectances in the Bahamas are currently being made by F.C. Polcyn under sponsorship of the Defense Mapping Agency (contract no. DMA 800-78-C-0060).

**When volume scattering is appreciable, the "effective" bottom reflectance defined by equation (8) must be used instead of the actual bottom reflectance. If the effective bottom reflectance is negative, as is possible in extreme cases of high scattering and low bottom reflectance, the X_i variables are not defined and the algorithm as formulated above is not applicable. However, a reformulation of the algorithm is possible to include these cases.

band i. These points may be projected onto a plane perpendicular to the direction defined by equation (15), thereby producing a new set of variables ($Y_1 \ldots Y_{n-1}$) which are independent of the water depth [10]. If $d \neq 0$, the two bottom types are theoretically separable at any depth if the system noise is sufficiently low.

This formulation depends upon the assumption that the radiance is a purely exponential function of the water depth (with an additive constant). Since there are effects which cause a deviation from this behavior, as discussed in section 2, the projected variables ($Y_1 \ldots Y_{n-1}$) are not completely depth-invariant even if the water optical properties are uniform throughout the scene. Therefore, an evaluation of the accuracy of this algorithm is necessary using a more detailed radiative transfer model which takes account of these effects. Such an evaluation is presented for two cases in sections 3.2 and 3.3.

3.2 EVALUATION IN CLEAR OCEANIC WATER

The first case considered is for Jerlov's oceanic water type IB (c.f. Figure 6) with bottom types consisting of sand and turtle grass (c.f. Figure 6). This set of parameters was chosen to model conditions occurring in the northwestern part of the Great Bahama Bank. Measurements of the irradiance attenuation coefficients in this area [8] have shown that the water is similar to Jerlov's water type IB, and observations of the bottom indicate that the most common bottom types in shallow water are sand and turtle grass (thalassia). In order to model the Landsat data for this area, radiances were calculated for the wavelength range from 0.5 μm to 0.7 μm and averaged over bands MSS4 (0.5-0.6 μm) and MSS5 (0.6-0.7 μm)*. The reflectances over a sand bottom as a function of depth were shown in Figure 3 of section 2.2. A plot of the radiances for MSS4 and MSS5, transformed as in equation (14), are shown in Figure 8 for the two bottom types. Although the X_i are not strictly linear functions of depth because of the effects described in section 2, only a small amount of nonlinearity is observed in Figure 8 because the effects in one band tend to cancel those in the other.

Since only two wavelength bands are considered, the transformation described in section 3.1 results in a single bottom-type index, which, for the parameters used in this example can be written as

$$Y_1 = 0.975 \ln(L_1 - L_{s1}) - 0.223 \ln(L_2 - L_{s2}) \qquad (17)$$

where L_1 is the radiance in MSS4 and L_2 is the radiance in MSS5. The values of Y_1 over sand and turtle grass are -0.98 and -2.11, respectively. Thus, a given sample would be classified as sand if the value of Y_1 is greater than -1.55, and as turtle grass if the value of Y_1 is less than -1.55. This is equivalent to drawing a decision boundary parallel to the two lines in Figure 8 and midway between them. Points falling above this boundary are classified as sand, and points below the boundary are classified as turtle grass.

In order to calculate the probabilities of misclassification of the bottom types in the presence of noise (which in this context includes the fluctuation in the observed signal due to surface reflections), a Monte Carlo procedure was used. At each depth, two sets of normally distributed random numbers were generated with mean values L_1 and L_2 and standard deviations of σ_1 and σ_2, where L_1 and L_2 are the radiances calculated from the model for the two bands and σ_1 and σ_2 are the noise-equivalent radiance values. The values of σ_1 and σ_2 were taken to be 0.01 mW cm^{-2} sr^{-1} based on the observed standard deviations of

---

*The model used for calculating these radiances is based on the quasi-single-scattering approximation, and includes the effects of internal reflection at the water surface. Atmospheric effects are also calculated using a double-delta approximation [11]. The atmospheric visibility assumed for this calculation was 23 km, and the solar zenith angle was 45°.

the Landsat deep-water signals for this area. For each of these randomly generated radiance pairs, the value of Y_1 is calculated and the bottom is classified as sand or turtle grass. If either radiance is less than the deep-water radiance, the sample is placed in the "unclassified" category. The probability of correct classification is the fraction of the random samples for a given category which are classified into the same category from which they were drawn.

The classification accuracies for sand and turtle grass are plotted versus depth in Figure 9. The depth at which the probability of misclassification reaches 50 percent is about 4 meters for turtle grass and 6.5 meters for sand. The classification errors are higher for turtle grass than for sand because the radiances are lower over turtle grass, so there is a higher probability of the radiance falling below the deep-water radiance in the presence of noise*. The noise equivalent radiance can be reduced by spatial filtering, at the cost of decreased spatial resolution. If a 2 x 2 pixel boxcar smoothing function is applied, the noise is reduced by a factor of two and the depths for 50 percent misclassification are increased to about 5 meters for turtle grass and 7.5 meters for sand. The irradiance attenuation length for MSS5 is about 3 meters for this water type, so the maximum depth for which turtle grass can be recognized with better than random accuracy is between 1 and 2 attenuation lengths, depending on the amount of noise in the data. These results have been generally confirmed with experimental data near North Cat Cay, which show accurate classification of turtle grass throughout the range of depths (1 to 4 meters) in which it was found to exist.

3.3 EVALUATION IN TURBID COASTAL WATER

The second case for which the bottom recognition algorithm has been evaluated is in water described by Jerlov's coastal type 5 attenuation coefficients (c.f. Figure 5). This case is intended to simulate the conditions occurring at a test site in St. Andrew Bay, Florida. Multispectral scanner data and a detailed set of subsurface observations were collected at this site, and an empirical evaluation of the bottom recognition algorithm was made comparing these observations with the results of processing the scanner data [12]. Four bottom types were observed in this scene including white sand, shoal grass, turtle grass, and a dark organic silt. Reflectances of the first three bottom types were measured in situ as was described in section 2.3 and plotted in Figure 6. The reflectance of the silt was not measured but was assumed, on the basis of the scanner data, to have a reflectance about half that of the sand. This assumed reflectance is also plotted as the dashed curve in Figure 6.

Multispectral scanner data were collected in several wavelengths bands, including the three bands centered at approximately 0.50 μm, 0.55μm and 0.65 μm which were selected for bottom recognition processing. Radiances were calculated for these bands in order to simulate the aircraft data set collected on 26 May 1977.** The transformed radiances in bands 1 and 2 are plotted versus the band 3 radiances in Figures 10a and 10b, respectively, for water depths ranging from 0 to 5 meters. In the X_1-X_3 plane (Figure 11a) the curves for turtle grass and shoal grass are nearly coincident, while in the X_2-X_3 plane (Figure 10b) the curves for shoal grass and silt are very close together. Probabilities of correct classification for these two wavelength pairs were calculated in the same manner as described in section 3.2 using a noise-equivalent radiance of 0.05 mW cm^{-2} sr^{-1} μm^{-1} for the aircraft scanner data. These results are plotted in Figures 11a and 11b. The relatively low classification accuracies for shoal grass and turtle grass in the first case, and for shoal grass and silt in the second case, are due to the closeness of the curves in Figure 10, as discussed above.

---

*Virtually all of the misclassification of turtle grass is into the "unclassified" category, with less than 2 percent being classified as sand at any depth.

**These radiances were calculated using the same model as in section 3.2. The solar zenith angle and atmospheric visibility were the same as in the earlier case, but the platform altitude was 300 meters instead of spacecraft altitude.

Next, the classification accuracy using all three bands was evaluated. In this case each data point is projected onto a plane perpendicular to the "depth axis", resulting in two depth-invariant indices Y_1 and Y_2. The projections onto this plane of the radiance values for each of the four bottom types are shown in Figure 12. The classification accuracy for a given bottom type is evaluated by generating random sets of radiance values for each band, calculating the values of Y_1 and Y_2 for each sample, and determining the distances from each sample to each of the "signatures" shown in Figure 12. The fraction of the random samples which are classified into the same category from which they were drawn is again the classification accuracy for that bottom type.

The results of these three-band calculations are shown in Figure 13. An interesting feature of this figure is the relative classification accuracy of shoal grass, as compared with the two-band results. In both two-band cases, shoal grass was the least accurately classified material. This was due to the proximity of the Y_1 value to that of turtle grass and the Y_2 value to that of silt. In the three-band case, however, the shoal grass signature is well separated from its neighbors and consequently the classification accuracy is much improved.

The average classification accuracy for the four bottom types is plotted in Figure 14 for the optimum two-band case (the 0.55/0.65 μm band pair) and for the three-band case. The average probability of correct classification is significantly improved in shallow water as the number of wavelength bands is increased from two to three, but the depth at which the accuracy equals that of a random guess (25 percent) remains about 3 meters. For deeper water, the probability of misclassification is actually larger for the three-band case because of the increased likelihood that one of the radiance values will fall below the deep-water radiance. The addition of a fourth band (0.60 μm) does not materially increase the classification accuracy in shallow water, and decreases it slightly in deeper water because of the above-mentioned effect. The irradiance attenuation length at 0.65 μm is about 2 meters, so the maximum depth for a better than random bottom classification accuracy is again between 1 and 2 attenuation lengths for the least penetrating wavelength band.

4. CONCLUSIONS

Theoretical modeling efforts have shown that the reflectance of shallow water can be approximately represented by a simple equation with two terms, the first being an exponential function of the water depth and the second an additive constant. Relatively small deviations from this simple exponential model are caused by volume scattering, internal reflection at the water surface, and selective absorption within the spectral bandwidth of the detector.

An algorithm for mapping bottom reflectance variations under a variable depth of water was proposed on the basis of the simple model described above and has been evaluated using a more complete model which includes the effects of scattering, internal reflection, and wavelength averaging. This theoretical evaluation indicates that bottom types such as sand and vegetation can be recognized to a maximum depth of one or two irradiance attenuation lengths for typical multispectral scanner systems. For relatively distinct bottom types, adequate results may be obtained with only two wavelength bands. For more subtle variations in bottom reflectance, the classification accuracy can be improved, within limits, by increasing the number of wavelength bands.

The advantage of a preliminary evaluation using a theoretical reflectance model is that feasibility can be demonstrated for a wide variety of environmental conditions and operational constraints at a relatively low cost. The reliability of such theoretical results depends not only upon the mathematical consistency of the model but upon the accuracy of the input parameters as well. More measurements of shallow-water optical properties and bottom reflectances are needed for a variety of coastal environments. Studies of the relationships among the physical and biological environments and the optical properties are also needed to improve the models and to develop new applications of remote sensing in shallow water areas. For example, large variations in bottom reflectance are caused by the growth of benthic vegetation, which is controlled by the availability of light and nutrients, the amount of wave action, and the type of

substrate. Variation of water parameters is due to land runoff, growth of phytoplankton, and resuspension of sediments by wave action on the bottom. Understanding the magnitude of these variations will allow a more accurate modeling of reflectance and may also lead to the use of remote sensing for making inferences about the environmental conditions which give rise to these variations.

ACKNOWLEDGEMENTS

This work was supported by the Office of Naval Research, Contract No. N00014-78-C-0458. Technical Monitor for this contract was Mr. Hans Dolezalek.

REFERENCES

1. G.W. Kattawar, T.J. Humphreys, and G.N. Plass, Radiative Transfer in an Atmosphere-Ocean System: A Matrix Operator Approach, Proc. Soc. Photo.-Opt. Instr. Eng., vol. 160, pp. 123-131, 1978.

2. H.R. Gordon and O.B. Brown, Influence of Bottom Depth and Albedo on the Diffuse Reflectance of a Flat Homogeneous Ocean, Applied Optics 13, 2153, 1974.

3. S.C. Jain and J.R. Miller, Subsurface Water Parameters: Optimization Approach to their Determination from Remotely Sensed Water Color Data, Applied Optics 15, 886, 1976.

4. H.R. Gordon, Simple Calculation of the Diffuse Reflectance of the Ocean, Applied Optics 12, 2803, 1973.

5. T.J. Petzold, Volume Scattering Functions for Selected Ocean Waters, Visibility Laboratory Tech. Report No. 72-78, Scripps Institute of Oceanography, San Diego, CA., 1972.

6. N.G. Jerlov, Optical Oceanography, Elsevier Pub. Co., Amsterdam, 1976.

7. John G. Shannon, Correlation of Beam and Diffuse Attenuation Coefficients Measured in Selected Ocean Waters, Proc. Soc. Photo.-Opt. Instrum. Eng., vol. 64, pp. 3-11, 1975.

8. F.C. Polcyn, NASA/Cousteau Ocean Bathymetry Experiment, ERIM Report No. 118500-1-F, 1976.

9. F. Thomson, R. Shuchman, C. Wezernak, D. Lyzenga, and D. Leu, Basic Remote Sensing Investigation for Beach Reconnaissance, ERIM Report No. 108900-5-P, 1976.

10. D.R. Lyzenga, Passive Remote Sensing Techniques for Mapping Water Depth and Bottom Features, Applied Optics 17, 379, 1978.

11. R.E. Turner, Radiative Transfer in Real Atmosphere, ERIM Report No. 190100-24-T, 1974.

12. D.R. Lyzenga, R.A. Shuchman, and R.A. Arnone, Evaluation of an Algorithm for Mapping Bottom Features Under a Variable Depth of Water, Proc. 13th International Symposium on Remote Sensing of Environment, 1979.

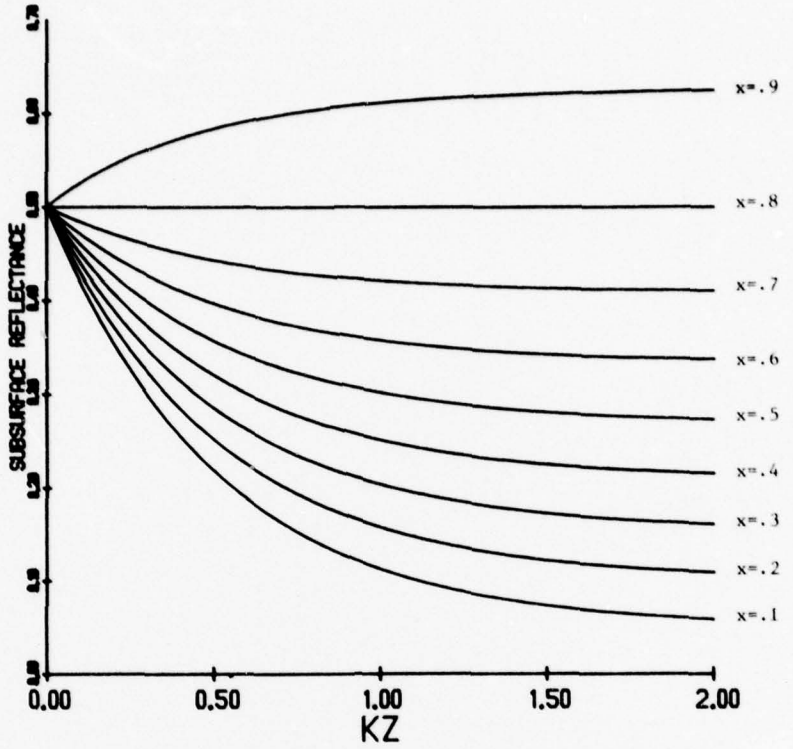

FIGURE 1. SUBSURFACE REFLECTANCE CALCULATED FROM TWO-STREAM APPROXIMATION FOR BOTTOM REFLECTANCE OF 50 PERCENT.

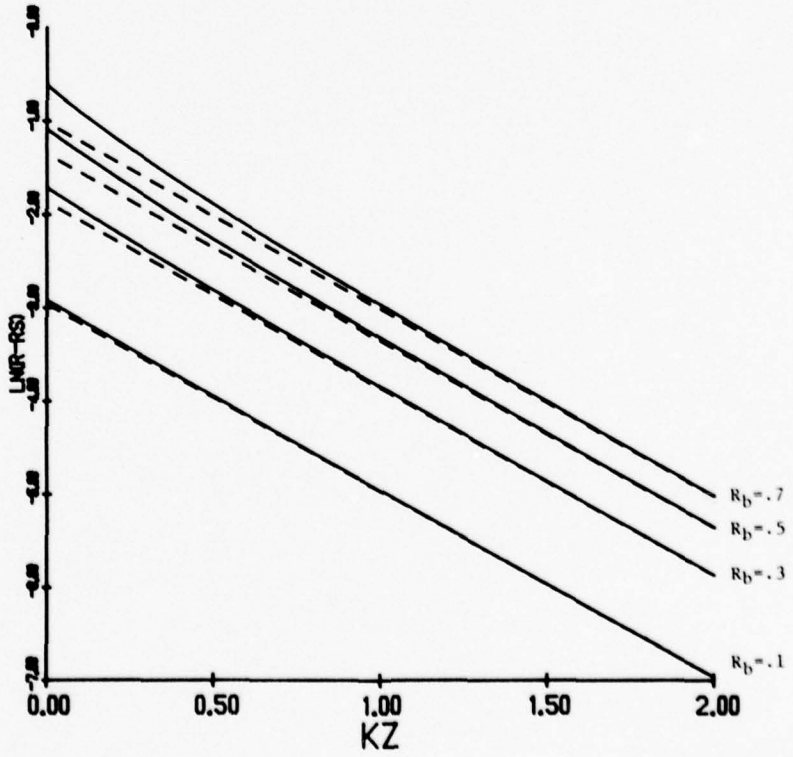

FIGURE 2. SHALLOW WATER REFLECTANCE INCLUDING INTERNAL REFLECTION EFFECTS (SOLID LINE) AND NEGLECTING THESE EFFECTS (DASHED LINE).

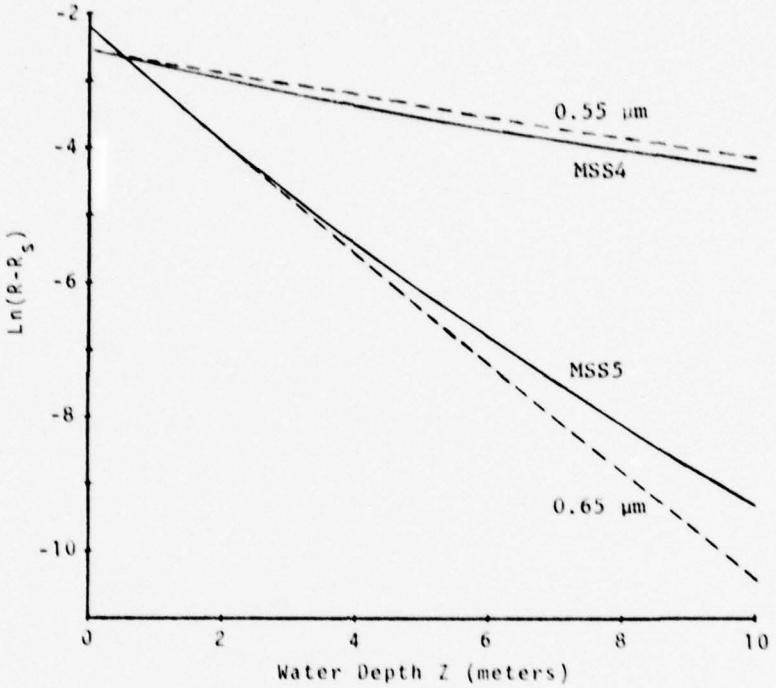

FIGURE 3. REFLECTANCE OF JERLOV WATER TYPE 1B WITH SAND BOTTOM IN LANDSAT BANDS MSS4 AND MSS5 (SOLID LINES) AND AT 0.55µm and 0.65 µm (DASHED LINES).

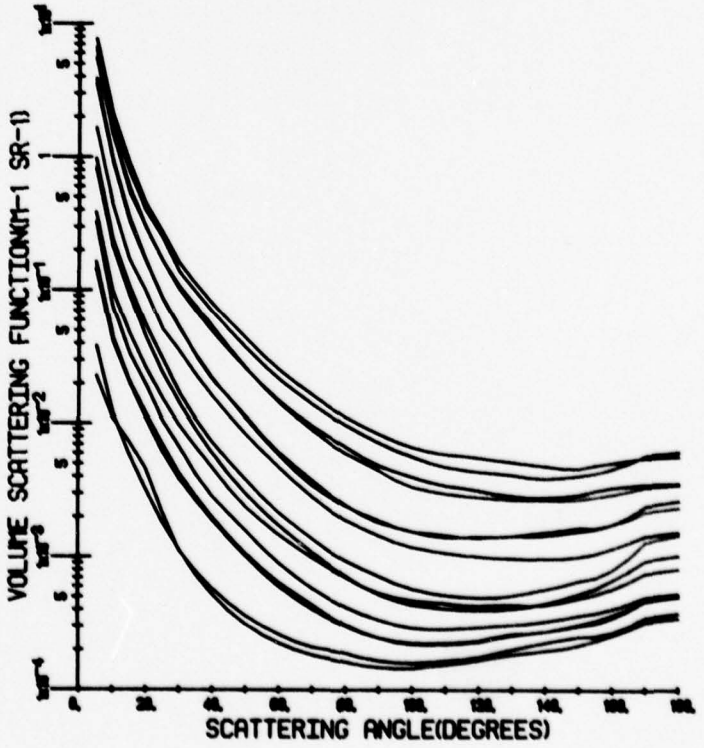

FIGURE 4. VOLUME SCATTERING FUNCTIONS MEASURED BY PETZOLD [5] FOR SELECTED OCEAN WATERS.

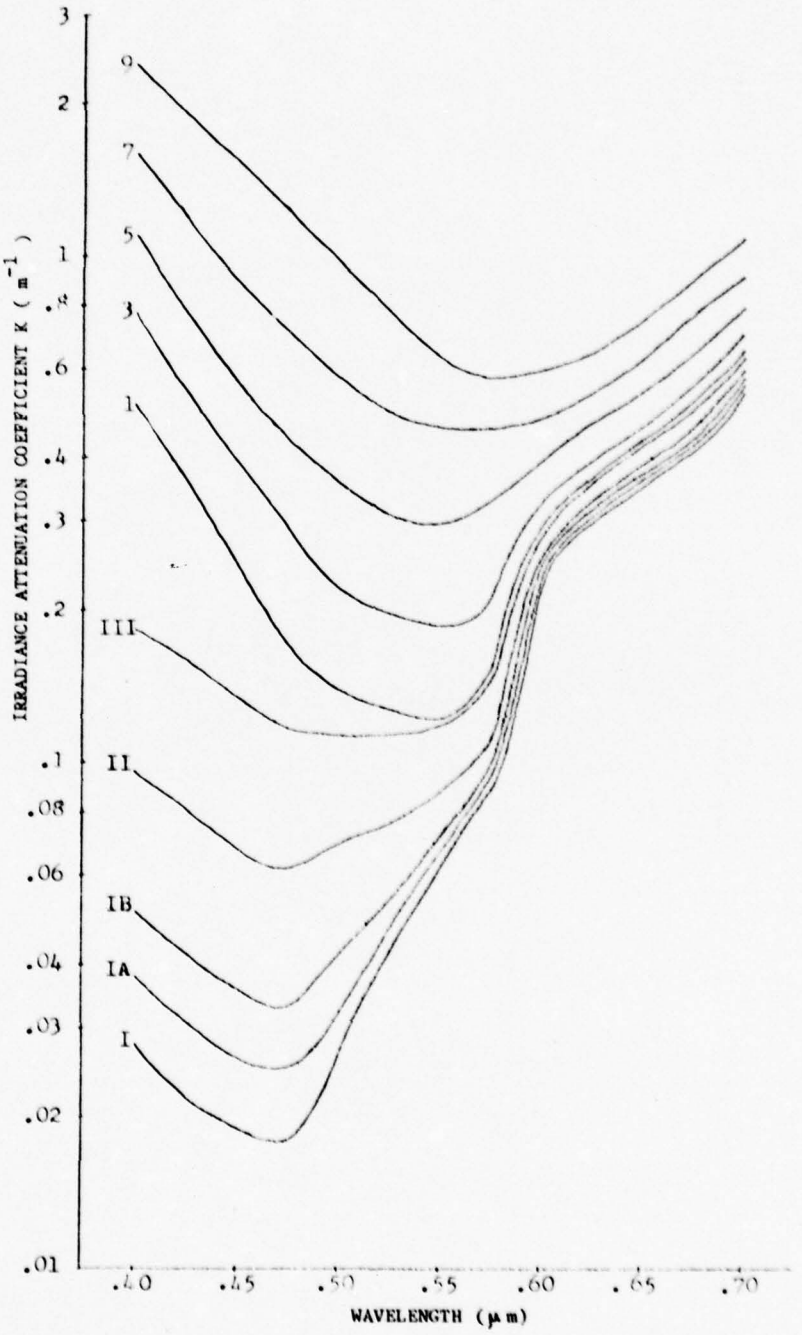

FIGURE 5. IRRADIANCE ATTENUATION COEFFICIENTS TABULATED BY JERLOV [6] FOR VARIOUS COASTAL AND OCEANIC WATER TYPES.

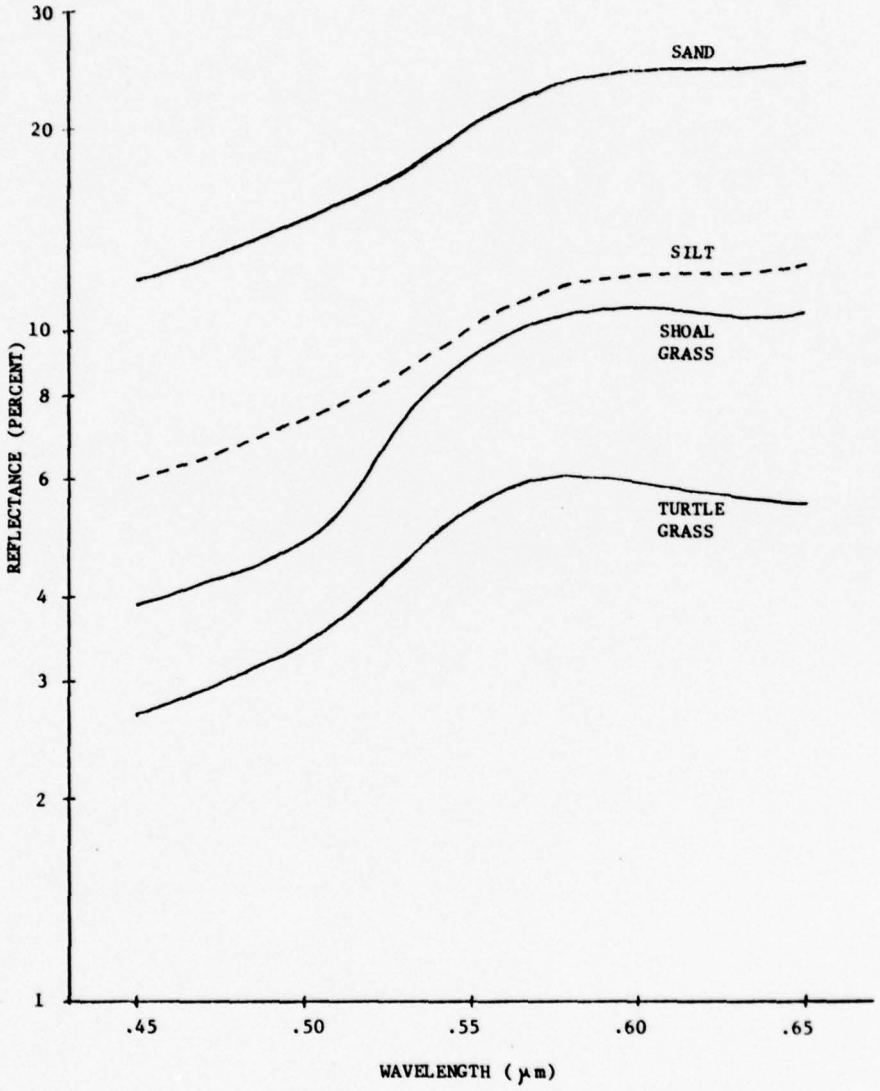

FIGURE 6. BOTTOM REFLECTANCES MEASURED FOR SAND, SHOAL GRASS, AND TURTLE GRASS IN ST. ANDREW BAY, FLORIDA. REFLECTANCE FOR SILT WAS INFERRED FROM SCANNER DATA.

FIGURE 7. PORTION OF LANDSAT FRAME 1925-15015 OVER THE NORTHWESTERN GREAT BAHAMA BANK. AREAS INDICATED BY ARROWS ARE AT DIFFERENT DEPTHS BUT HAVE APPROXIMATELY THE SAME MSS4 RADIANCE BECAUSE OF DIFFERENCES IN BOTTOM REFLECTANCE.

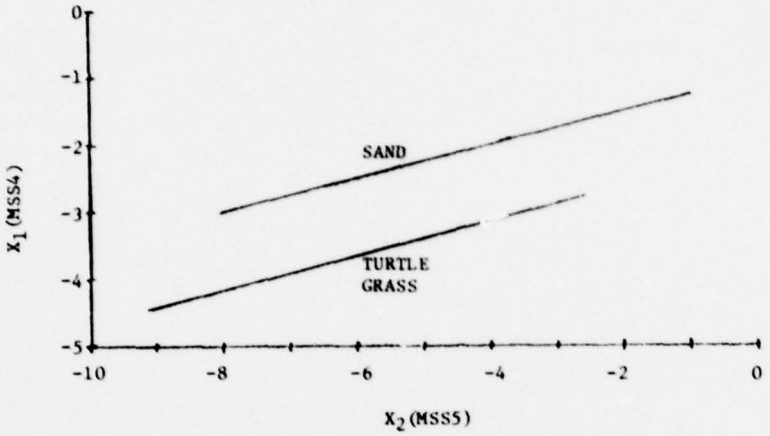

FIGURE 8. PLOT OF X_1 (MSS4) VERSUS X_2 (MSS5) FOR SAND AND TURTLE GRASS IN JERLOV WATER TYPE IB, WITH DEPTH RANGING FROM 0 TO 10 METERS.

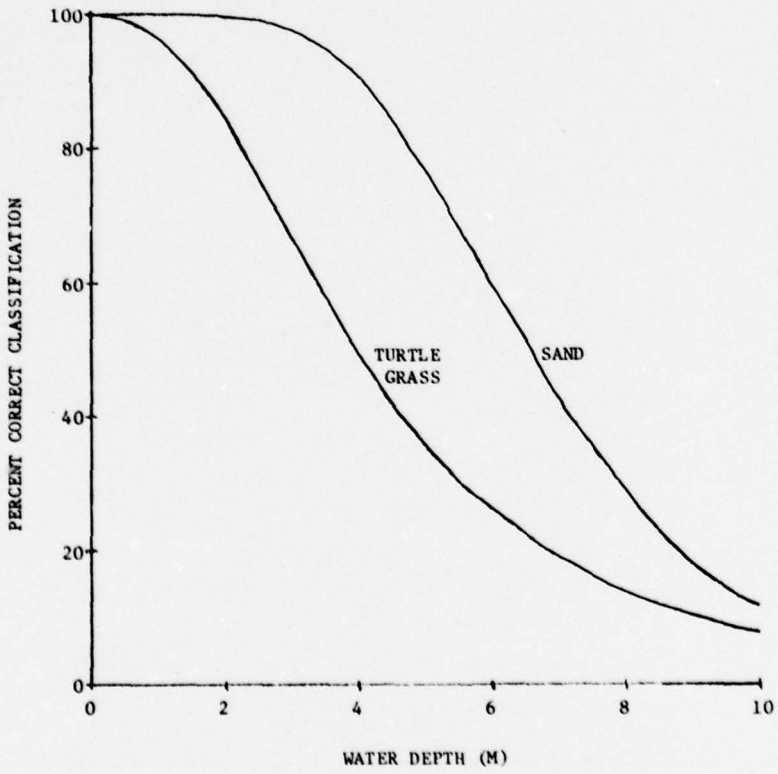

FIGURE 9. CLASSIFICATION ACCURACIES FOR SAND AND TURTLE GRASS IN JERLOV WATER TYPE IB.

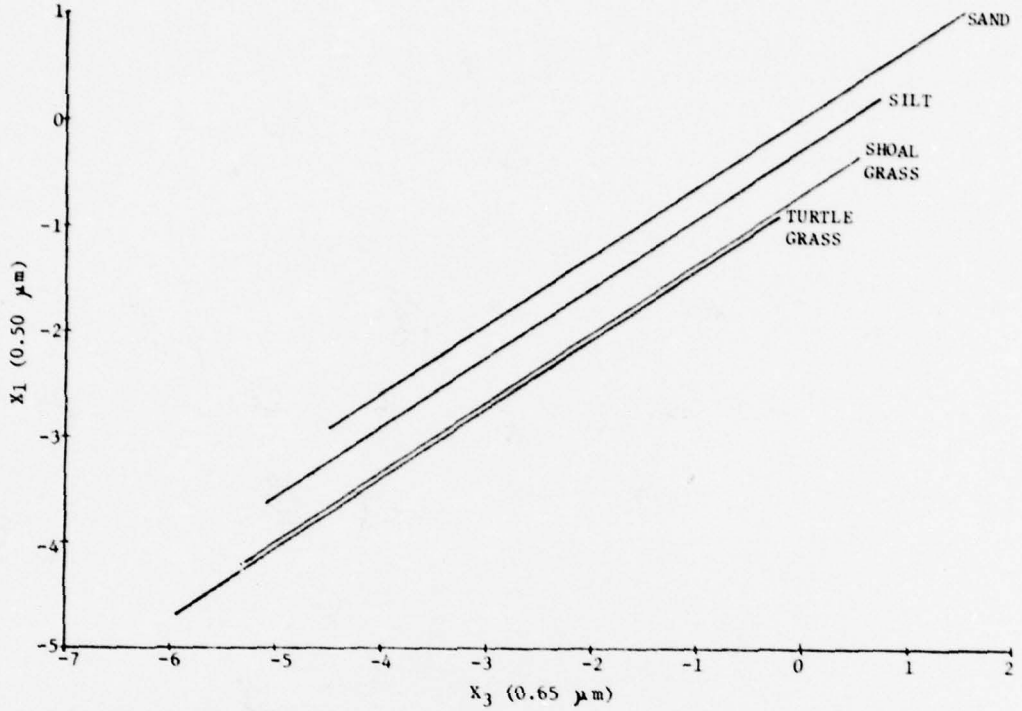

FIGURE 10a. PLOT OF X_1 (.50 μm) VERSUS X_3 (.65 μm) FOR FOUR BOTTOM TYPES IN JERLOV WATER TYPE 5, WITH DEPTH RANGING FROM 0 TO 5 METERS.

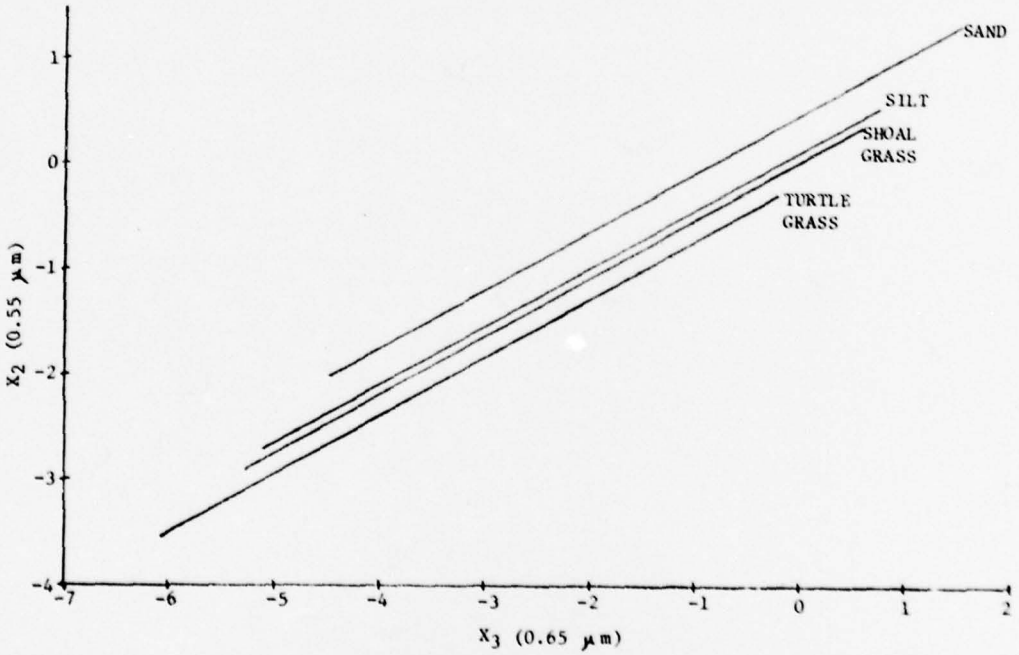

FIGURE 10b. PLOT OF X_2 (.55 μm) VERSUS X_3 (.65 μm) FOR FOUR BOTTOM TYPES IN JERLOV WATER TYPE 5, WITH DEPTH RANGING FROM 0 TO 5 METERS.

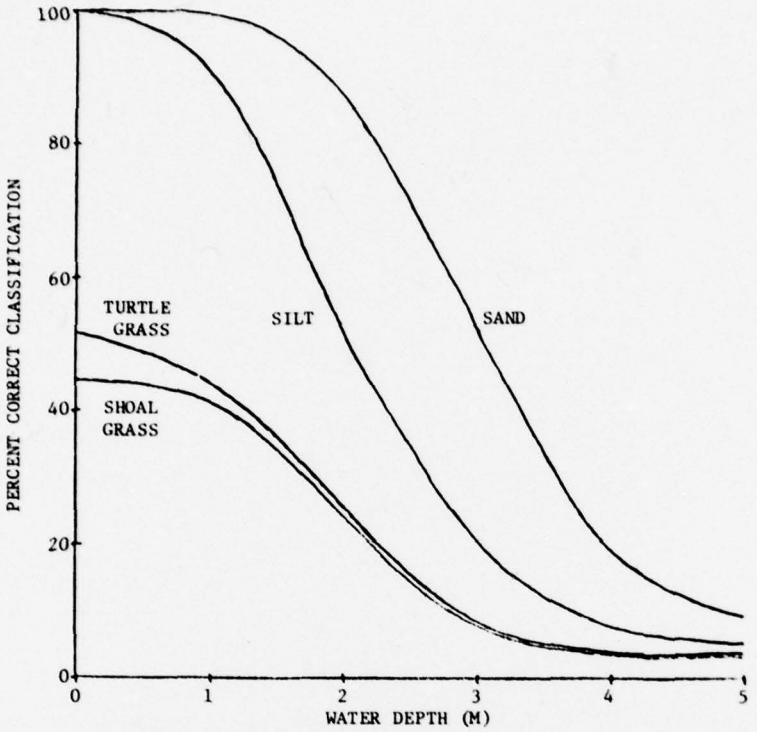

FIGURE 11a. CLASSIFICATION ACCURACIES FOR FOUR BOTTOM TYPES IN JERLOV WATER TYPE 5, USING 0.50/0.65 μm BAND PAIR.

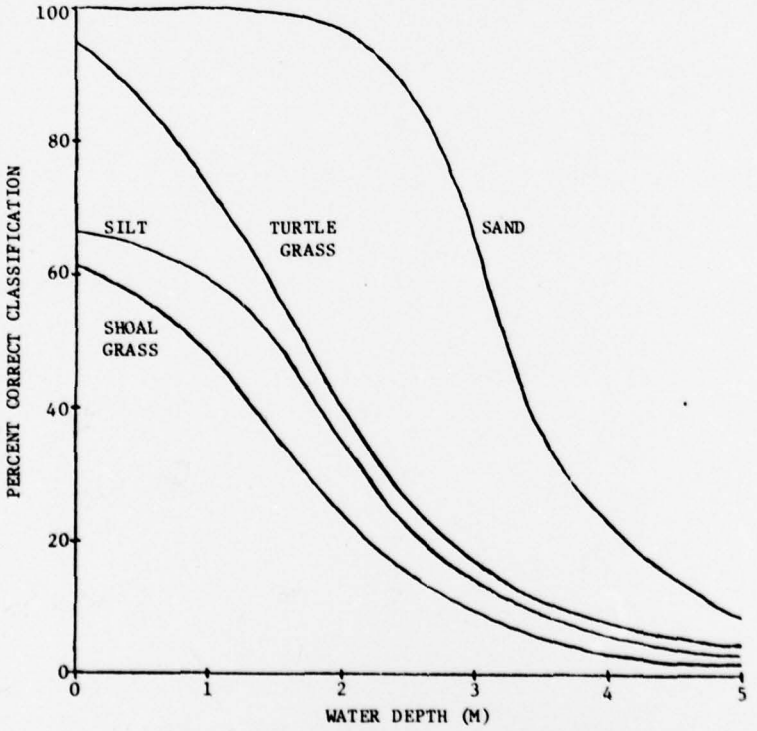

FIGURE 11b. CLASSIFICATION ACCURACIES FOR FOUR BOTTOM TYPES IN JERLOV WATER TYPE 5, USING 0.55/0.65 μm BAND PAIR.

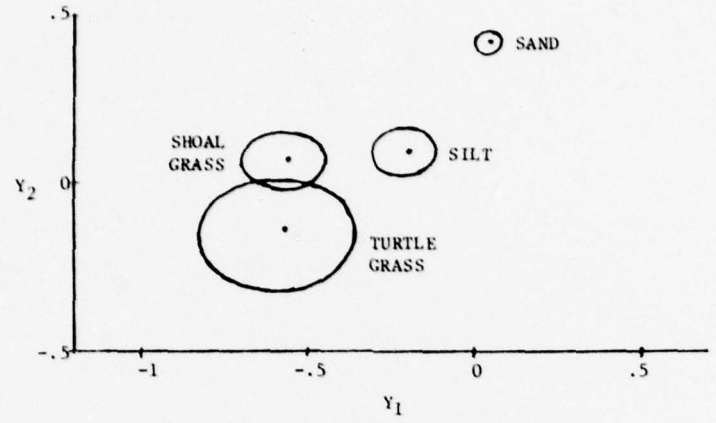

FIGURE 12. DEPTH-INVARIANT "SIGNATURES" FOR FOUR BOTTOM TYPES IN JERLOV WATER TYPE 5. CLOSED CURVES INDICATE STANDARD DEVIATION OF SIGNALS AT 1 METER DEPTH.

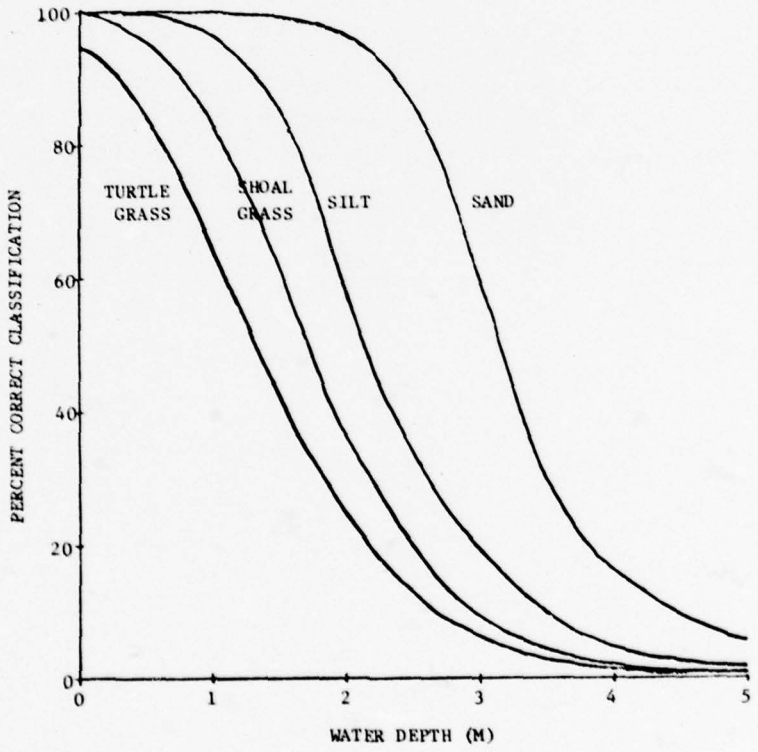

FIGURE 13. CLASSIFICATION ACCURACIES FOR FOUR BOTTOM TYPES IN JERLOV WATER TYPE 5, USING THREE INPUT WAVELENGTH BANDS.

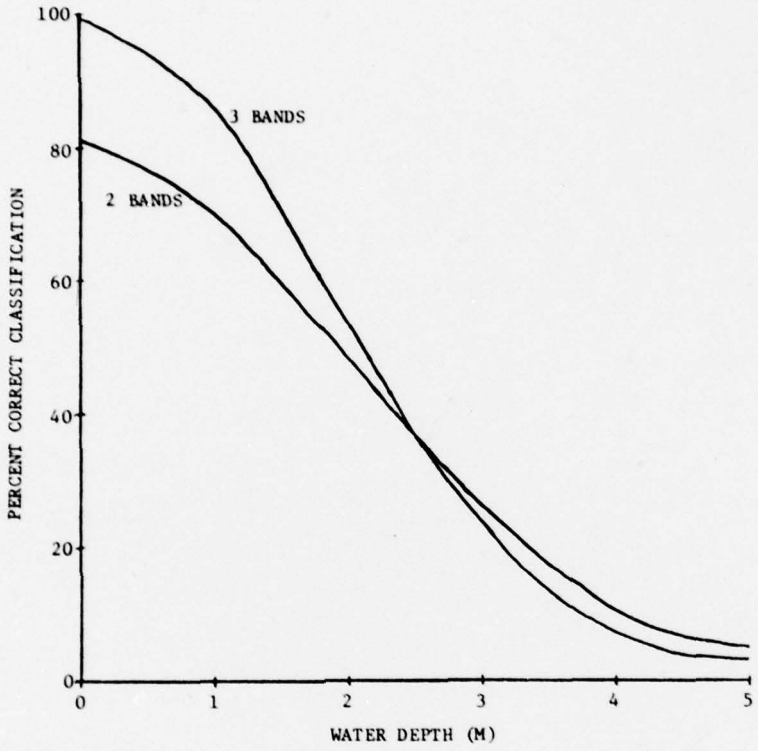

FIGURE 14. AVERAGE CLASSIFICATION ACCURACIES FOR FOUR BOTTOM TYPES IN JERLOV WATER TYPE 5 USING TWO AND THREE WAVELENGTH BANDS.

UNCLASSIFIED

SECURITY CLASSIFICATION OF THIS PAGE *(When Data Entered)*

REPORT DOCUMENTATION PAGE		READ INSTRUCTIONS BEFORE COMPLETING FORM
1. REPORT NUMBER 134400-/-T (Part 3)	2. GOVT ACCESSION NO.	3. RECIPIENT'S CATALOG NUMBER
4. TITLE *(and Subtitle)* EVALUATION OF AN ALGORITHM FOR MAPPING BOTTOM FEATURES UNDER A VARIABLE DEPTH OF WATER		5. TYPE OF REPORT & PERIOD COVERED TECHNICAL REPORT 3/1/78 to 2/28/79 6. PERFORMING ORG. REPORT NUMBER 134400-7-T
7. AUTHOR*(s)* D.R. Lyzenga, R.A. Shuchman, and R.A. Arnone		8. CONTRACT OR GRANT NUMBER*(s)* N00014-78-C-0458
9. PERFORMING ORGANIZATION NAME AND ADDRESS Environmental Research Institute of Michigan P.O. Box 8618, APPLICATIONS DIVISION Ann Arbor, MI 48107		10. PROGRAM ELEMENT, PROJECT, TASK AREA & WORK UNIT NUMBERS Marine Environment Task
11. CONTROLLING OFFICE NAME AND ADDRESS Geography Branch Office of Naval Research Arlington, VA 22217		12. REPORT DATE April 1979 13. NUMBER OF PAGES 14
14. MONITORING AGENCY NAME AND ADDRESS *(if different from Controlling Office)*		15. SECURITY CLASS *(of this report)* Unclassified 15a. DECLASSIFICATION/DOWNGRADING SCHEDULE
16. DISTRIBUTION STATEMENT *(of this Report)* Distribution of this document is unlimited.		
17. DISTRIBUTION STATEMENT *(of the abstract entered in Block 20, if different from Report)*		
18. SUPPLEMENTARY NOTES This report was presented at the Thirteenth International Symposium on Remote Sensing of Environment, April 23-27, 1979.		
19. KEY WORDS *(Continue on reverse side if necessary and identify by block number)* Remote Sensing Multispectral Scanner Data Processing		
20. ABSTRACT *(Continue on reverse side if necessary and identify by block number)* Conventional maximum-likelihood classification techniques do not accurately map bottom features under a variable depth of water, because of the variance in the spectral signatures of the bottom introduced by attenuation in the water. A processing technique has been developed for reducing the variance in the bottom signatures by removing the effects of attenuation in the water column. This technique is described, and its accuracy is		

DD FORM 1 JAN 73 1473 EDITION OF 1 NOV 65 IS OBSOLETE

UNCLASSIFIED

SECURITY CLASSIFICATION OF THIS PAGE *(When Data Entered)*

20. ABSTRACT (Continued)

evaluated using an aircraft data set and surface-truth observation in St. Andrew Bay, Florida.

A test area of 150m by 180m was surveyed by divers and the bottom was classified into 10 categories, including sand, silt, shoal grass, turtle grass, and various mixtures. Multispectral scanner data for the same area was processed to produce a four-category bottom map utilizing two and three input channels. The average classification accuracy was found to be 58 percent using the two input channels and 65 percent using three input channels. For a two-category classification, the average classification accuracy is 76 percent using two input channels and 83 percent using three input channels.

EVALUATION OF AN ALGORITHM FOR MAPPING BOTTOM FEATURES UNDER A VARIABLE DEPTH OF WATER

D. R. Lyzenga
R. A. Shuchman

Environmental Research Institute of Michigan
Ann Arbor, Michigan

R. A. Arnone

Naval Coastal Systems Center
Panama City, Florida

ABSTRACT

Conventional maximum-likelihood classification techniques do not accurately map bottom features under a variable depth of water, because of the variance in the spectral signatures of the bottom introduced by attenuation in the water. A processing technique has been developed for reducing the variance in the bottom signatures by removing the effects of attenuation in the water column. This technique is described, and its accuracy is evaluated using an aircraft data set and surface-truth observations in St. Andrew Bay, Florida.

A test area of 150m by 180m was surveyed by divers and the bottom was classified into 10 categories, including sand, silt, shoal grass, turtle grass, and various mixtures. Multispectral scanner data for the same area was processed to produce a four-category bottom map utilizing two and three input channels. The average classification accuracy was found to be 58 percent using the two input channels and 65 percent using three input channels. For a two-category classification, the average classification accuracy is 76 percent using two input channels and 83 percent using three input channels.

1. INTRODUCTION

The subject of this paper is the empirical evaluation of a proposed algorithm for the recognition and classification of bottom types under a variable depth of water. The primary motivation for the development of this algorithm was to improve the accuracy of water depth calculations from multispectral scanner data; however, the technique has potential applications to geological and biological studies of shallow-water areas as well. A specialized technique for recognizing bottom types under water is necessary because the variance in the bottom signatures induced by absorption and scattering in the water column prevents the use of conventional multispectral classification techniques.

The evaluation was carried out at a test site in St. Andrew Bay, Florida. Detailed subsurface observations were made in the 150m by 180m test site and a multispectral scanner data set was collected at low altitude using the ERIM

M-8 scanner*. This data set was processed to produce bottom-type maps of the area using two and three wavelength bands, and the results were compared with the subsurface observations on a point-by-point basis. Discrimination of four bottom types was attempted, including sand, silt, shoal grass, and turtle grass. Water optical properties at the test site were similar to Jerlov's Coastal Water type 5. Because of the relatively high water attenuation and the number of bottom types in the scene, this situation probably represents a limiting case for which the technique is applicable.

2. TEST SITE DESCRIPTION

The test site for this evaluation was in St. Andrew Bay, near the Naval Coastal Systems Center in Panama City, Florida. This is an inland bay which is fed by several small creeks and discharges through a narrow outlet to the Gulf of Mexico. Fresh water coming from these creeks contains high concentrations of humic and tannic acid, resulting in relatively poor visibility. The test site is located on the west side of the Bay near the NCSC Marina, and includes a narrow channel leading into the Marina. The maximum depth in the test site is approximately 2.5 meters, which corresponds to roughly one-irradiance attenuation length (i.e. 1/K, where K is the maximum irradiance attenuation coefficient for the water).

2.1 SUBSURFACE OBSERVATIONS

A 150 by 180 meter area centered about the NCSC marina channel was selected for detailed subsurface and water measurements. During the week prior to 25 May 1977 a grid system was set up within the test area and detailed observations of the bottom types and the water depth were made at the grid points. The depth measurements were processed on a Hewlett Packard Programmable Calculator 9825 and used to generate a contour plot of the bottom topography [1]. The bottom-type observations were organized into six basic categories plus four mixtures of these categories. The six basic bottom types observed in the test site were:

(1) clean white quartz sand
(2) thin shoal grass (<7.5 cm long)
(3) thick shoal grass (>7.5 cm long)
(4) thin turtle grass (<15 cm long)
(5) thick turtle grass (>15 cm long)
(6) dark organic silty sand

Representative underwater photographs of sand, shoal grass, and turtle grass taken at the test site on 26 May 1977 are shown in Figure 1. The bottom observations were summarized in the form of a second chart showing the distribution of bottom types in the test area [1]. These observations indicate that shoal grass occurs primarily in the 0.5 - 1.0 meter depth range while the turtle grass grows mostly in water deeper than 1 meter. Sand occurs near the shoreline in less than 0.5 meters of water and in scattered patches at all depths. The silt category was observed only in the bottom of the marina channel.

On the 25th and 26th of May, 1977 a set of measurements of water optical properties were also made at various points within the test site. Most of these measurements were made with a beam transmissometer, but some measurements of the irradiance attenuation coefficient were also made. The transmissometer measured beam attenuation coefficients on the order of 1.5 - 2.0 m^{-1}, from which

---

*The M-8 scanner records the scene radiance in eight spectral bands in the visible and near IR regions. The spatial resolution is 2.5 milliradians and the scan rate is 60 per second. The instrument also incorporates two laser illuminations and detection systems, but this capability was not utilized during the present study.

a range of irradiance attenuation coefficients from 0.3 - 0.4 m^{-1} was inferred using the relationship reported by Shannon [2]. This relationship was generally confirmed by spot measurements of irradiance attenuation at other locations. Maximum water transmission was observed for wavelengths around 0.57 μm due to the high concentrations of "yellow substance" in the bay. These observations characterize the water as being similar to Jerlov's water type 5 [3].

These observations were carried out under a program organized by the Naval Coastal Systems Center (NCSC) to evaluate the use of remote sensing techniques for coastal reconnaissance [1, 4]. The primary focus of this program was on water depth mapping, rather than bottom feature extraction. During the present study some of the data collected as a part of this program was re-analyzed for the specific purpose of evaluating a multichannel bottom recognition algorithm which was not fully developed at the time of the original program. In order to facilitate a comparison between the bottom-type observations and the results of processing the aircraft data set (c.f. section 2.2), the bottom-type map was converted into a digital file. This file consists of a set of 200 by 240 pixels, each corresponding to an area of 0.75m by 0.75m on the bottom. A number representing the bottom type is stored at each pixel location. A display of this digital file is shown in Figure 2. In this display the two shoal grass categories have been combined together, as have the two turtle grass categories. Sand and silt are shown separately, and the various mixture categories are indicated by the cross-hatched areas.

2.2 MULTISPECTRAL SCANNER DATA SET

Multispectral scanner data was collected over the NCSC test site with the ERIM M-8 scanner system on the morning of 26 May, 1977. The platform altitude was 300 meters and the speed was about 45 meters/sec, resulting in a spatial resolution and pixel size of about 0.75 meters. The solar zenith angle was about 45 degrees at the time of the overflight. Data was collected in the eight wavelength bands indicated in Table 1. An image display of the data in band 4 (.52-.57 μm) is shown in Figure 3.

This data was collected under the NCSC bathymetry experiment mentioned in Section 2.1, and was processed to produce water depth charts as part of that program [4]. During the present study, this data set was re-processed using a newly developed multichannel bottom recognition algorithm. The details of this processing are discussed in the following sections.

3. BOTTOM RECOGNITION PROCESSING

The algorithm which was used for processing the aircraft data set was proposed earlier [5] and has been theoretically evaluated for the same set of conditions as encountered in this test [6]. Briefly, the steps involved in the bottom recognition processing algorithm are: (1) subtracting the deep-water signals, (2) calculating the natural logarithm of the signals after deep-water subtractions, (3) taking linear combinations of these logarithms in order to create a set of N-1 depth-invariant signal channels from the original set of N data channels, and (4) using these depth-invariant signals as inputs to a conventional multispectral classification routine in order to categorize the bottom types.

Prior to the first step in this sequence, two pre-processing steps were carried out on the NCSC data set. The first was a spatial filtering, or smoothing, to reduce the noise in the data. The second step was to edit out land areas using a threshold value in the near-infrared band (band 8), which has a high reflectance over land and a low reflectance over water. The deep-water signals were obtained by averaging a set of scan lines in the along-track direction, so as to obtain the deep-water signal as a function of the pixel number or scan angle. The sequence of steps outlined above was then

carried out using subsets of two and three input wavelength bands. Details and results of this processing are described in the following sections.

3.1 TWO-BAND RESULTS

The first test of the algorithm was made using two input wavelength bands. The bands selected for processing were bands 4 (.52-.57 μm) and 7 (.62-.70 μm). The second step in the sequence outlined above yields the variables

$$X_1 = \ln (V_1 - Vs1) \tag{1}$$

and

$$X_2 = \ln (V_2 - Vs2) \tag{2}$$

where V_1 is the data value in band 4, Vs1 is the deep-water signal in band 4, and V_2 and Vs2 are the corresponding values for band 7. A plot of the relative frequency of occurrence of these variables is shown in Figure 4. These variables are approximately linear functions of the water depth. Thus, a change in the water depth causes a displacement of the data points for a given bottom type along the direction indicated by the straight line in Figure 4. The data points in this figure fall into two main groups corresponding to sand and turtle grass, which together constitute about 70 percent of the total scene area. A projection of the data points onto a line perpendicular to the direction indicated on Figure 4 yields the depth-invariant index

$$Y_1 = 0.740\ X_1 - 0.673\ X_2 \tag{3}$$

which has an average value of 0.07 over sand, -0.47 over silt, -0.54 over shoal grass, and -0.70 over shoal grass. Since there is only one depth-invariant index of bottom type for this case, the fourth step in the processing sequence reduces to a simple threshold criterion on the value of this index. The results of this processing are displayed in Figure 5.

Next, a detailed pixel-by-pixel comparison was made between the subsurface observations of the bottom type (Figure 2), and the two-band bottom recognition map (Figure 5). In order to simplify the presentation, the two shoal grass categories were combined into a single category, as were the two turtle grass categories. The mixed bottom types were ignored for this comparison. The number of pixels classified into each recognition category were then calculated separately for each observed bottom type. The results of this calculation are shown in Table 2. The probabilities of correct classification are 81.8 percent for sand, 61.7 percent for turtle grass, 52.3 percent for silt, and 35.4 percent for shoal grass. The average classification accuracy for the four bottom types is 57.8 percent, as compared with a value of 25 percent for a purely random guess. The low classification accuracy of silt and shoal grass is due to the small difference in the Y1 values for these materials which is in turn due to the similarity in the reflectances of these materials. Shoal grass has a thin blade structure which has a relatively small projected area when viewed vertically, and is also frequently covered with small bubbles and organic detritus which makes its color similar to the silt observed in the channel. If a less ambitious classification of the bottom types into two categories ("vegetated" versus "non-vegetated") is attempted, the classification accuracies are higher, as shown in Table 3. The average classification accuracy for this case is 75.8 percent, as compared with 50 percent for a random guess. These results are in fair agreement with the theoretically predicted classification accuracies [6] for an average depth of about 1.5 meters.

3.2 THREE-BAND RESULTS

In order to evaluate the effect of increasing the number of operating wavelength bands, the bottom recognition processing was repeated using three bands, including band 2 (.48-.52 μm) in addition to the two bands used earlier. In this case, two depth-invariant indices, Y1 and Y2 are generated from the three input data values for each pixel. A plot of the frequency of occurrence of each (Y1, Y2) pair in the test site is shown in Figure 6. In this case a set of decision boundaries in two-space must be used for the bottom classification. These decision boundaries are also indicated in Figure 6.

The bottom-type map generated from the three channel algorithm is shown in Figure 7. This map shows a much clearer differentiation between the silt category in the channel and the shoal grass outside of the channel. This improved differentiation is also reflected in the statistics shown in Table 4. The classification accuracy for silt has increased to 64.6 percent, and that for shoal grass has increased to 52.2 percent, while the figures for sand and turtle grass have remained virtually unchanged. The theoretical evaluation [6] predicted a somewhat larger increase in the classification accuracies of silt and shoal grass, along with a small decline in the classification accuracy of turtle grass which did not occur in the experimental data, although such a phenomenon might have occurred if the decision boundaries had been shifted slightly toward the turtle grass signature.

The average classification accuracy for the four bottom categories using the three-band algorithm is 65.1 percent, as compared with 57.8 percent for the two-band case. The frequency of classification of each of the observed bottom types into the combined "vegetated" and "non-vegetated" categories are shown in Table 5. The average probability of correct classification into these two categories is 82.7 percent for the three-band case, as compared with 75.8 percent for the two-band case.

4. CONCLUSIONS

The two-band bottom recognition algorithm described in this report gives satisfactory classification accuracies for distinct bottom types such as sand and turtle grass in water depths ranging from zero to about one attenuation length. The probabilities of correct classification are in excess of 90 percent when only these two categories are considered. When the classification scheme is extended to include bottom types which are less distinct, such as shoal grass and dark organic silt, the average classification accuracy falls to 57.8 percent for four categories and 75.8 percent for two categories. The inclusion of a third wavelength band increases the classification accuracies of silt and shoal grass considerably, resulting in an average probability of correct classification of 65.1 percent for four categories and 82.7 percent for two categories. These observed classification accuracies are comparable to those predicted using a theoretical water reflectance model.

ACKNOWLEDGEMENTS

The surface truth data and aircraft data were originally collected under the sponsorship of the Naval Coastal Systems Center (contract N61339-77-C-0059). Subsequent analysis of this data was funded by the Office of Naval Research (contract N00014-78-C-0458). Technical monitor for the ONR contract was Mr. Hans Dolezalek.

REFERENCES

1. R. A. Arnone, Ground Truth Analysis of Multispectral/Laser System Experiment, NCSC Technical Memorandum No. TM240-78, September 1978.

2. John G. Shannon, Correlation of Beam and Diffuse Attenuation Coefficients Measured in Selected Ocean Waters, Proc. Soc. Photo-Opt. Instrum. Eng., Vol. 64, pp. 3-11, 1975.

3. N. G. Jerlov, Marine Optics, Elsevier Pub. Co., Amsterdam, 1976.

4. R. A. Shuchman and D. R. Lyzenga, Active-Passive Scanner Bathymetry and Land Feature Classification Results, ERIM Report No. 128500-4-T, March 1978.

5. D. R. Lyzenga, Passive Remote Sensing Techniques for Mapping Water Depth and Bottom Features, Applied Optics 17, 379-383, 1978.

6. D. R. Lyzenga, Shallow Water Reflectance Modelling with Applications to Remote Sensing of the Ocean Floor, Proc. 13th Intl. Symposium on Remote Sensing of Environment, 1979.

TABLE 1. MULTISPECTRAL SCANNER WAVELENGTH BANDS

Band	Wavelength (μm)
1	.46-.49
2	.48-.52
3	.50-.54
4	.52-.57
5	.55-.60
6	.58-.64
7	.62-.70
8	1.5-1.8

TABLE 2. FOUR-CATEGORY CLASSIFICATION STATISTICS FOR BOTTOM RECOGNITION ALGORITHM WITH TWO INPUT BANDS

Observed Bottom Type	% Recognized as Sand	Silt	Shoal Grass	Turtle Grass
Sand	81.8	10.1	7.7	0.4
Silt	0.1	52.3	47.4	0.2
Shoal Grass	5.2	28.9	35.4	30.5
Turtle Grass	0.2	6.9	31.2	61.7

TABLE 3. TWO-CATEGORY CLASSIFICATION STATISTICS FOR BOTTOM RECOGNITION ALGORITHM WITH TWO INPUT BANDS

Observed Bottom Type	% Recognized as Non-vegetated	Vegetated
Sand	91.9	8.1
Silt	52.4	47.6
Shoal Grass	34.1	65.9
Turtle Grass	7.1	92.9

TABLE 4. FOUR-CATEGORY CLASSIFICATION STATISTICS FOR BOTTOM RECOGNITION ALGORITHM WITH THREE INPUT BANDS

Observed Bottom Type	% Recognized as Sand	Silt	Shoal Grass	Turtle Grass
Sand	81.8	6.4	10.8	1.0
Silt	0.1	64.6	34.1	1.2
Shoal Grass	5.3	13.5	52.2	29.0
Turtle Grass	0.2	3.0	34.9	61.9

TABLE 5. TWO-CATEGORY CLASSIFICATION STATISTICS FOR BOTTOM RECOGNITION ALGORITHM WITH THREE INPUT BANDS

Observed Bottom Type	% Recognized as Non-vegetated	Vegetated
Sand	88.2	11.8
Silt	64.7	35.3
Shoal Grass	18.8	81.2
Turtle Grass	3.2	96.8

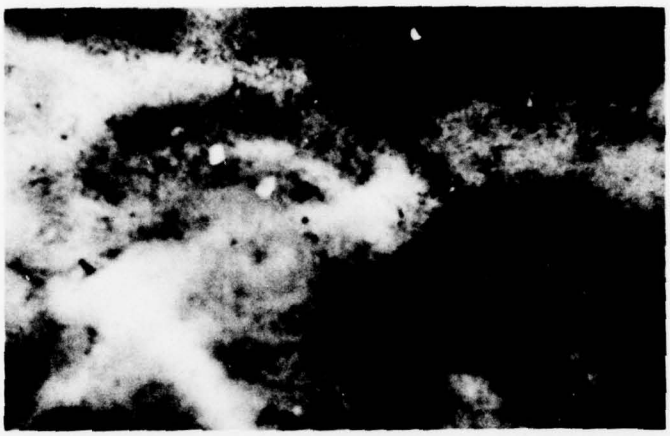

(a) Sand

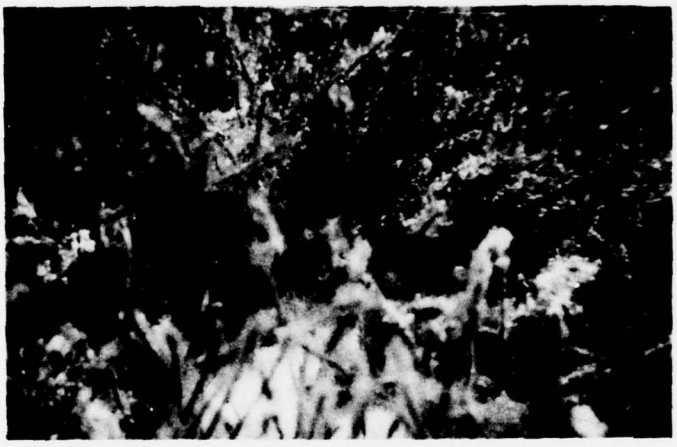

(b) Shoal Grass

(c) Turtle Grass

FIGURE 1. UNDERWATER PHOTOGRAPHS OF SAND, SHOAL GRASS, AND TURTLE GRASS TAKEN IN ST. ANDREW BAY, FLORIDA.

FIGURE 2. DIGITAL BOTTOM-TYPE MAP FOR TEST AREA COMPILED FROM SUBSURFACE OBSERVATIONS.

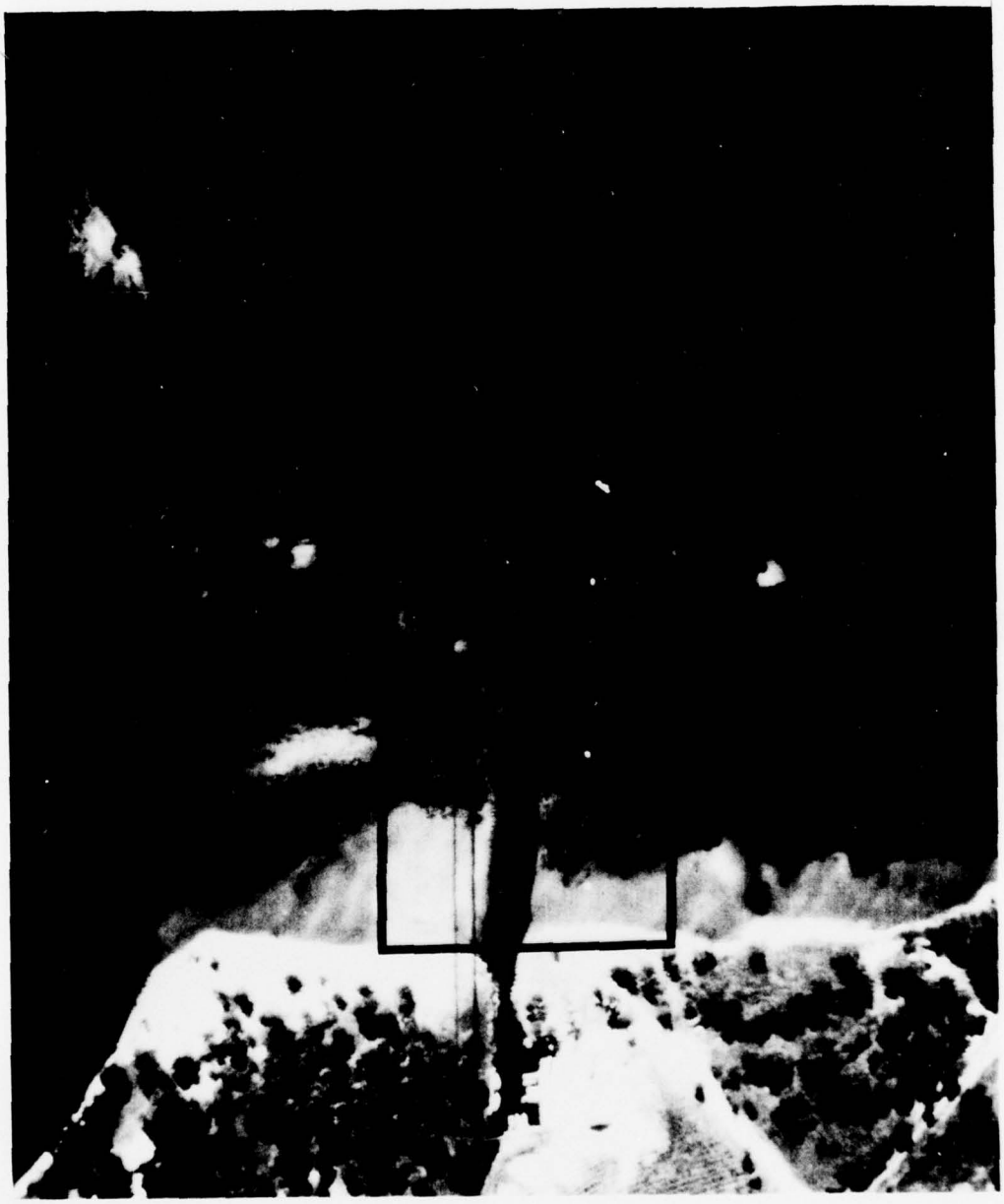

FIGURE 3. DISPLAY OF SCANNER DATA IN BAND 4 (.52-.57 μm) OVER TEST AREA.

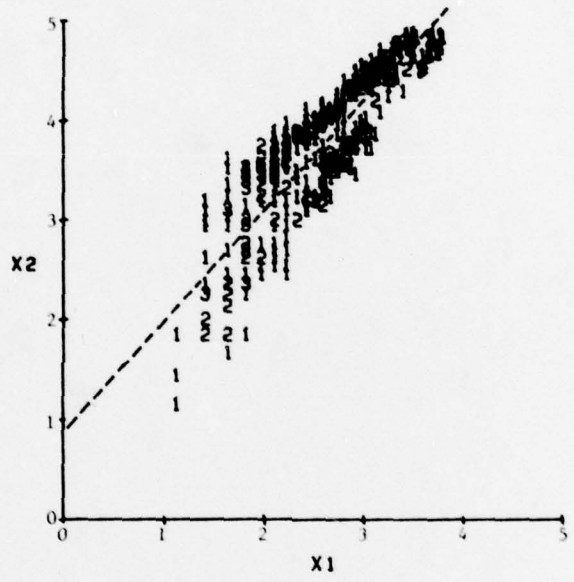

FIGURE 4. TWO-DIMENSIONAL SCATTER PLOT OF TRANSFORMED RADIANCE VALUES (X_1 AND X_2) IN TEST AREA. DASHED LINE INDICATES DIRECTION OF DISPLACEMENT DUE TO WATER DEPTH VARIATIONS.

FIGURE 5. BOTTOM-TYPE MAP GENERATED FROM TWO-BAND ALGORITHM

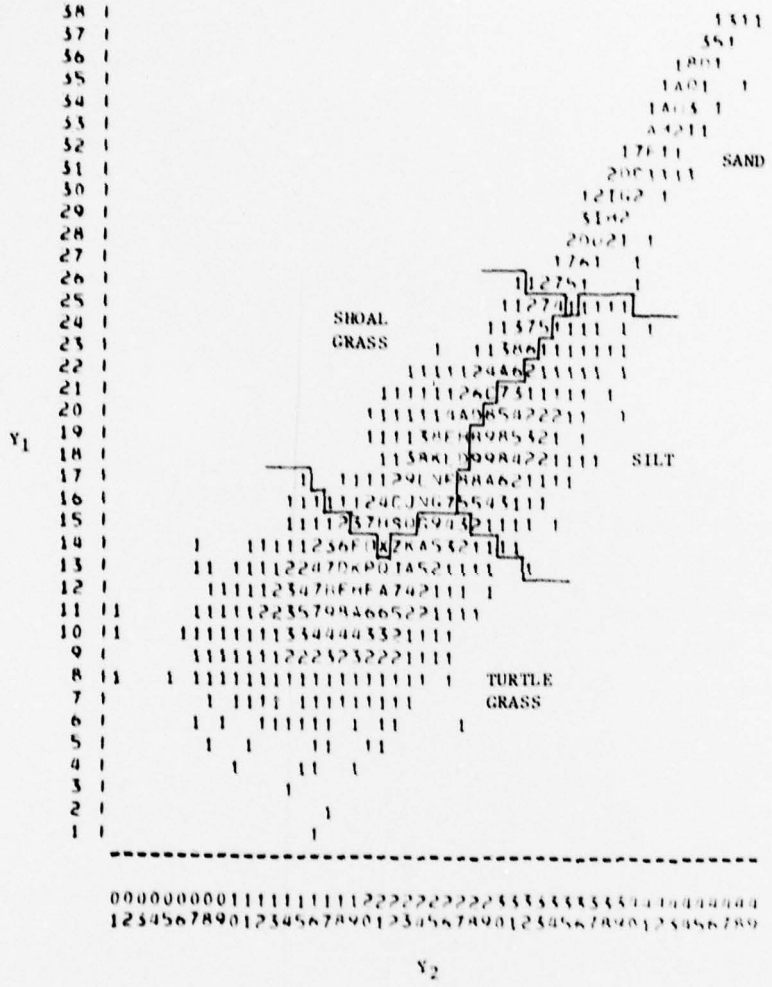

FIGURE 6. TWO-DIMENSIONAL SCATTER PLOT OF DEPTH-INVARIANT BOTTOM INDICES (Y_1 AND Y_2) IN TEST AREA. LINES INDICATE DECISION BOUNDARIES FOR BOTTOM CLASSIFICATION.

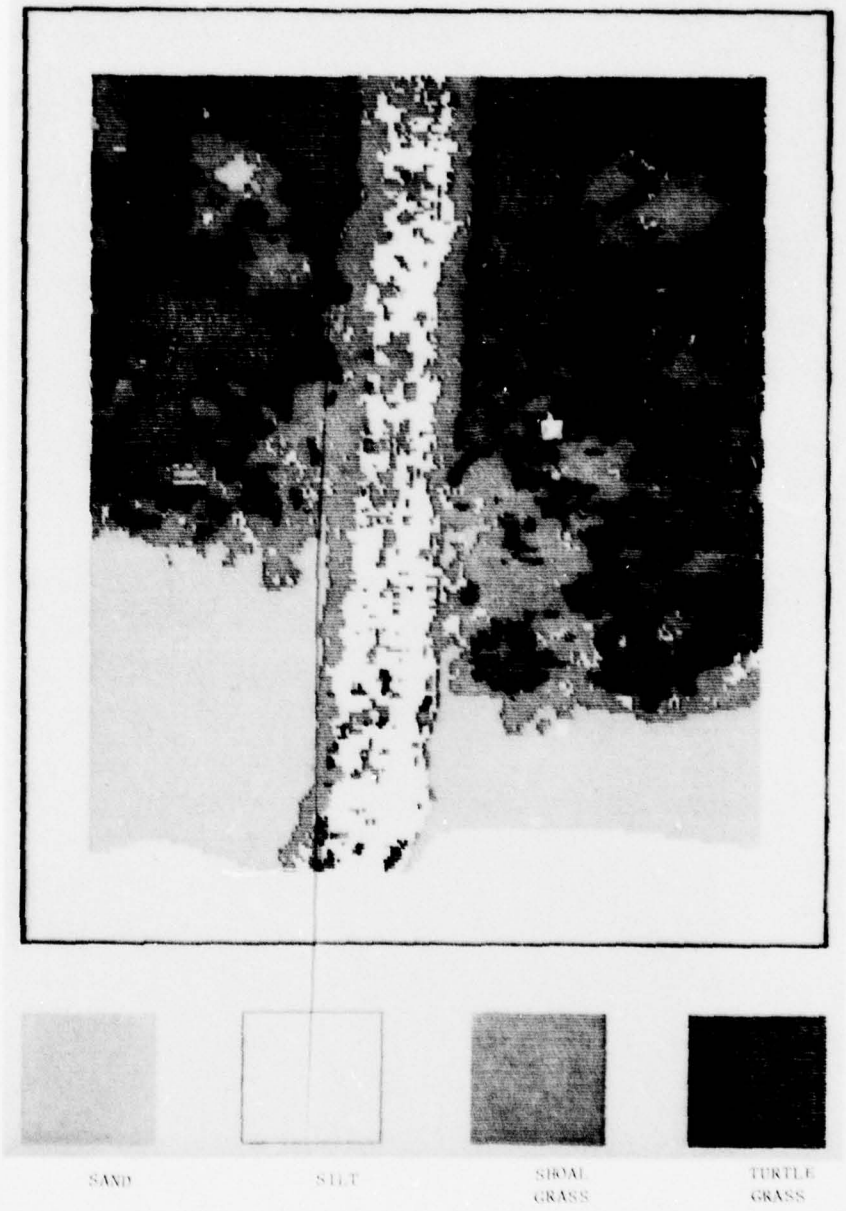

FIGURE 7. BOTTOM-TYPE MAP GENERATED FROM THREE-BAND ALGORITHM.

ERIM

DISTRIBUTION LIST

Office of Naval Research
Geography Programs
Code 462
Arlington, Virginia 22217

Defense Documentation Center — 12 copies
Cameron Station
Alexandria, Virginia 22314

Director, Naval Research Lab — 6 copies
Attention: Technical Information Officer
Washington, D.C. 20375

Director,
Office of Naval Research Branch Office
1030 East Green Street
Pasadena, California 91101

Director,
Office of Naval Research Branch Office
536 South Clark Street
Chicago, Illinois 60605

Director,
Office of Naval Research Branch Office
495 Summer Street
Boston, Massachusetts 02210

Commanding Officer
Office of Naval Research Branch Office
Box 39
FPO New York 09510

Chief of Naval Research
Asst. for Marine Corps Matters
Code 100M
Office of Naval Research
Arlington, Virginia 22217

NORDA
Code 400
National Space Technology Laboratories
Bay St. Louis, Mississippi 39520

Office of Naval Research
Operational Applications Division
Code 200
Arlington, Virginia 22217

Office of Naval Research
Scientific Liaison Officer
Scripps Institution of Oceanography
La Jolla, California 92093

Director, Naval Research Laboratory
Attention: Library, Code 2628
Washington, D.C. 20375

2 copies — ONR Scientific Liaison Group
American Embassy - Room A-407
APO San Francisco 96503

Commander
Naval Oceanographic Office
Attention: Library Code 1600
Washington, D.C. 20374

Naval Oceanographic Office
Code 3001
Washington, D.C. 20374

Chief of Naval Operations
OP 987P1
Department of the Navy
Washington, D.C. 20350

Oceanographer of the Navy
Hoffman II Building
200 Stovall Street
Alexandria, Virginia 22322

Naval Academy Library
U.S. Naval Academy
Annapolis, Maryland 21402

Commanding Officer
Naval Coastal Systems Laboratory
Panama City, Florida 32401

Librarian
Naval Intelligence
Support Center
4301 Suitland Road
Washington, D.C. 20390

Officer in Charge
Environmental Research Prdctn. Fclty.
Naval Postgraduate School
Monterey, California 93940

Commanding General
Marine Corps Development and Educational Command
Quantico, Virginia 22134

Dr. A. L. Slafkosky
Scientific Advisor
Commandant of the Marine Corps
Code MC-RD-1
Washington, D.C. 20380

Defense Intelligence Agency
Central Reference Division
Code RDS-3
Washington, D.C. 20301

Director
Defense Mapping Topographic Center
Attention: Code 50200
Washington, D.C. 20315

Commanding Officer
U.S. Army Engineering
Topographic Laboratory
Attention: ETL-ST
Fort Belvoir, Virginia 22060

Chief, Wave Dynamics Division
USAE-WES
P.O. Box 631
Vicksburg, Mississippi 39180

National Oceanographic Data
Center D764
Environmental Data Services
NOAA
Washington, D.C. 20235

Central Intelligence Agency
Attention: OCR/DD-Publications
Washington, D.C. 20505

Dr. Mark M. Macomber
Advanced Technology Division
Defense Mapping Agency
Naval Observatory
Washington, D.C. 20390

Ministerialsrat Dr. F. Wever
RUE/FO
Bundesministerium der Verteidigung
Hardthoehe
D-5300 Bonn, West Germany

Oberregierungsrat Dr. Ullrich
Rue/FO
Bundesministerium der Verteidigung
Hardthoehe
D-5300 Bonn, West Germany

Mr. Tage Strarup
Defence Research Establishment
Osterbrogades Kaserne
DK-2100 Koberhavn O, Denmark

IR. M. W. Van Batenberg
Physisch Laboratorium INO
Oude Wallsdorper Weg 63, Den Haag
Netherlands

Dr. Gordon E. Carlson
University of Missouri
Department of Electrical Engineering
Rolla, Missouri 65401

Coastal Studies Institute
Louisiana State University
Baton Rouge, Louisiana 70803

Dr. Bernard Le Mehaute
Tetra Tech. Inc.
630 North Rosemead Boulevard
Pasadena, California 91107

Dr. William S. Gaither
Dean, College of Marine Studies
Robinson Hall
University of Delaware
Newark, Delaware 19711

Dr. Lester A. Gerhardt
Rennsselaer Polytechnic Institute
Troy, New York 12181

Dr. Thomas K. Peucker
Simon Fraser University
Department of Geography
Burnaby 2, B.C., Canada

Dr. Bruce Hayden
Department of Environmental Sciences
University of Virginia
Charlottesville, Virginia 22903